THE UNIVERSITY OF ALBERTA

BENDING BEHAVIOUR OF BI-TRAPEZOIDAL PLATES

by

M. GARY FAULKNER, B.Sc. (Alberta)

A THESIS

SUBMITTED TO THE FACULTY OF GRADUATE STUDIES

IN PARTIAL FULFILMENT OF THE REQUIREMENTS FOR THE DEGREE

OF MASTER OF SCIENCE

DEPARTMENT OF MECHANICAL ENGINEERING

EDMONTON, ALBERTA

JANUARY 1966

UNIVERSITY OF ALBERTA

FACULTY OF GRADUATE STUDIES

The undersigned certify that they have read, and recommend to the Faculty of Graduate Studies for acceptance, a thesis entitled "BENDING BEHAVIOUR OF BI-TRAPEZOIDAL PLATES" submitted by M. GARY FAULKNER in partial fulfilment of the requirements for the degree of Master of Science.

ACKNOWLEDGEMENTS

The author wishes to express his appreciation and thanks to

- Dr. D.G. Bellow for suggesting the research topic and supervising the thesis
- the members of the Mechanical Engineering shop and particularly Ray Marak who did the strain gauge bonding and instrumentation
- Mrs. Cathy Arial for patience and attention in typing the thesis
- the University of Alberta Computing Center for their help in program preparation
- my wife, Maxine, for her continued understanding and patience.

ABSTRACT

The problem of determination of the transverse deflections of plates under conditions of pure bending in the longitudinal direction is considered for plates with a bi-trapezoidal transverse cross section. Previous investigators have considered the transverse deflections of plates with rectangular and double-wedge shaped cross sections. This thesis extends this work to include the case of a bi-trapezoidal cross section. With a suitable change of parameters, the developed theory is shown to approach both these known results.

Experiments carried out on two bi-trapezoidal plates showed that the developed theory agreed quite closely with the experimental results. The discrepancies between experiment and theory which occurred at large longitudinal curvatures were attributed to the initial imperfections in the plate.

CONTENTS

FIGURES

[illegible]

Figure | Page

[illegible]

[illegible] [illegible]

[illegible] [illegible] [illegible]

[illegible] [illegible]

NOTATION

b	-	one-half the plate width
c	-	thickness of the longitudinal edges
E	-	modulus of elasticity
e_x, e_y, e_z	-	normal strains in the x,y and z-directions
h_m	-	one-half maximum plate thickness $= t_o + c/2$
k	-	non-dimensional coefficient defined in figure 1.3
M_x, M_y	-	bending moments per unit distance
N_x, N_y	-	normal forces per unit distance
Q_x, Q_y	-	shearing forces per unit distance
R	-	radius of curvature of the neutral surface in the longitudinal direction
R_x, R_y	-	radii of curvature of the middle surface in the direction of the subscript
t_i	-	thickness of the plate at a point x_i
t_o	-	one-half thickness of the tapered portion of the plate as shown in figure 1.3
v	=	$\zeta^* \sqrt{\gamma}$
w	-	deflection of the midline of the cross section in the z-direction measured from the centroidal axis
w_o	-	initial deflection of the cross section measured from the centroidal axis
x, y, z	-	rectangular coordinates as shown in figure 1
α	=	$2\lambda(1+\beta)^{1/2}$
β	=	$c/2t_o$
γ	=	$\xi + \beta = \rho/2$
ϵ	=	$2\lambda\beta^{1/2}$

ζ - distortion of the midline of the cross section due to the applied loads

$= \zeta^* + \zeta_o$ - complimentary function and particular integral

η $= 2\lambda(1 - \frac{x}{b} + \beta)^{1/2}$

$\theta_1, \theta_2, \theta_3, \theta_4$ - real and imaginary parts of the two independent solutions of the differential equation

λ^2 $= b^2\left[3(1-\mu^2)\right]^{1/2} / Rt_o$

μ - Poisson's ratio

ξ $= 1 - \frac{x}{b}$

ρ $= t/t_o$

σ_x, σ_y - normal stresses in the x and y directions

ψ $= \eta\sqrt{i}$ where $i = \sqrt{-1}$

INTRODUCTION

When a beam whose width is the same order of magnitude as its depth, is bent into a uniform longitudinal curvature $1/R$, the transverse curvature is $-\mu/R$ producing an anticlastic surface. This is provided the longitudinal edges are free. When the width of the beam is large compared to its depth the transverse curvature is restrained in the central portion of the transverse section, however, the edges of the section are seen to curl. The bending behaviour of wide beams or plates has received considerable attention in the literature. Theoretical work has been presented by Lamb(1) and Ashwell(2) while experimental verification of Lamb's(1) theory has been given by Bellow, Ford and Kennedy(3), and Conway and Nickola(4). These investigators, as well as others, have shown the mode of deformation to depend on the ratio b^2/Rt where b is the beam or plate width and t is the thickness.

The problem is complicated, however, when plates having a tapered transverse cross section are considered. Plates with various tapered cross sections have been investigated theoretically by Flugge(5), Murray and Niles(6), Fung and Wittrick(7) and Conway and Farnham(8). The aim of this thesis is to extend the work of the above authors and to consider both theoretically and experimentally the transverse behaviour of plates having a bi-trapezoidal cross

[illegible]

[illegible]

[illegible]

section. The plate orientation and a general bi-trapezoidal cross section are shown in figures 1 and 2.

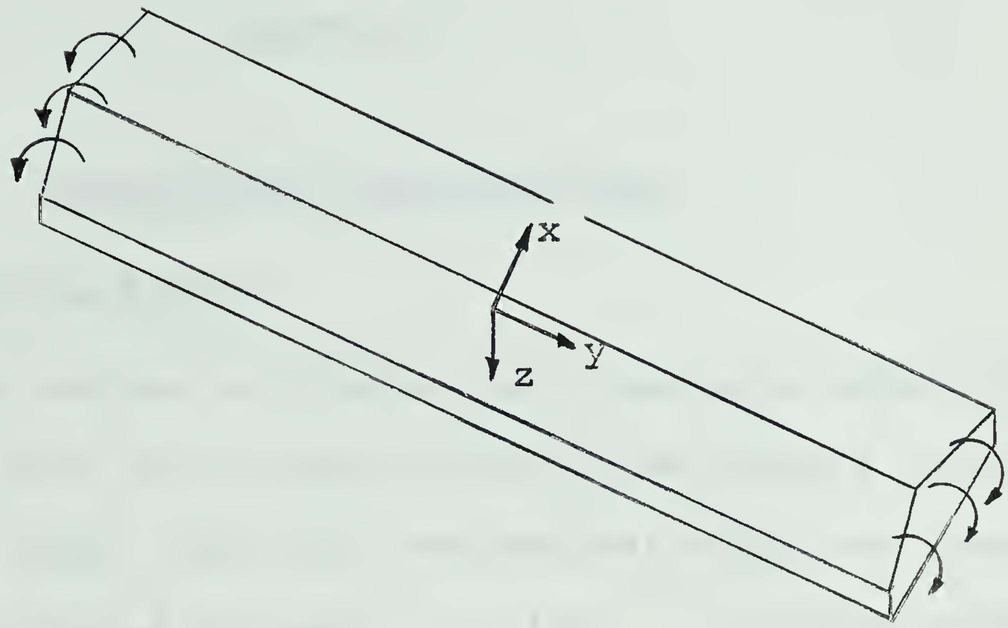

FIGURE 1. PLATE ORIENTATION

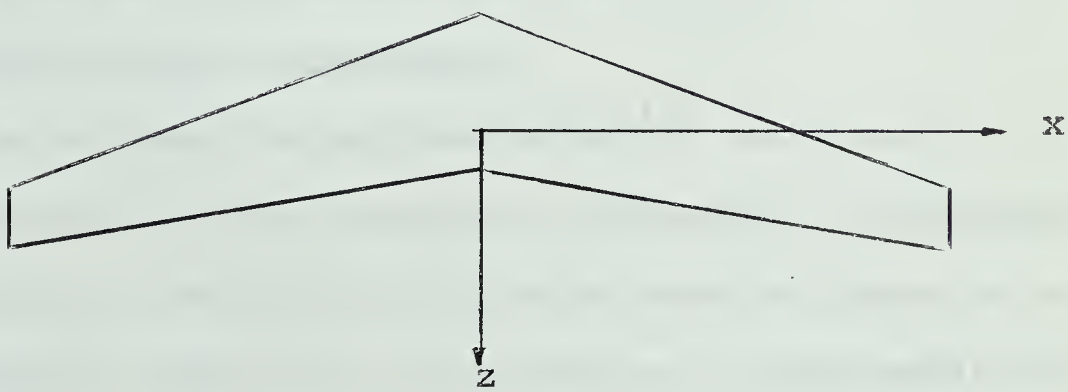

FIGURE 2. GENERAL BI-TRAPEZOIDAL CROSS SECTION

CHAPTER I

THEORETICAL CONSIDERATIONS

1.1 Historical Review

The problem of finding the transverse deflections of a plate bent by uniformly distributed moments on its transverse edges, when the longitudinal edges are free, was first investigated by Lamb[1] in 1891. His development of the governing differential equation, which considered the equilibrium of a small plate element, is used in this thesis.

In analyzing problems with similar boundary and loading conditions, Flugge[5] in 1949, derived a differential equation which accounted for a thickness variation in the transverse direction. This work included results which showed the transverse deflections for rectangular, diamond and certain bi-trapezoidal sections for various values of longitudinal curvature.

Also in 1949, Murray and Niles[6] developed a graphical method and its numerical equivalent to determine the anticlastic curvature of any wide beam or plate of an arbitrary doubly symmetric solid section. This numerical method was used to calculate the transverse deflection curves for rectangular, diamond and bi-convex cross sections.

Fung and Wittrick[7] in 1954 developed the govern-

[illegible]

ing differential equation with allowance for a transverse thickness variation using the large deflection equations of Von Karman. The solution of the differential equation and results for various double-wedge shapes were shown.

Recently Conway and Farnham[8], in 1964, solved the governing equation for a transverse cross section which had a central uniform section and edge sections which tapered in a parabolic curve to form an infinitely thin edge.

The governing differential equation, which is developed below for the transverse deflections of a bi-trapezoidal plate, is completely analogous to the deflections of a cylindrical tank with a linearly varying wall thickness. The tank problem has been analyzed by Timoshenko[9] and Flugge[10].

1.2 Development of the Theoretical Solution.

1.2-1 Lamb's Development

Consider the plate shown in figure 1. It is subjected to a longitudinal curvature produced by uniformly distributed moments M_y applied along the edges which lie in the x-z plane. The x-z plane contains the transverse cross section.

The following assumptions were made:

1. The behaviour of the plate under loading is perfectly elastic and obeys Hooke's law.
2. The material is isotropic and homogeneous.
3. The slope of the transverse deflection curve is small compared to unity.
4. The weight of the plate is negligible compared to the applied forces.

Consider the equilibrium of the plate element shown in figure 1.1. The x and y-axes are chosen to be principal axes so that the forces and moments are principal valued. Force equilibrium parallel to the x-axis gives

$$\left[N_x + \frac{\partial N_x}{\partial x} \cdot dx \right] dy - N_x dy = 0$$

therefore $\dfrac{\partial N_x}{\partial x} = 0$ and $N_x = f(y)$.

At the edges $x = \pm b$ there are no surface forces. It follows that N_x must be zero at these edges and all across the transverse section.

$$N_x = 0 \qquad 1.2\text{-}1$$

Force equilibrium parallel to the y-axis shows that N_y must be a constant value.

$$\sum F_z = 0$$

$$\left[Q_x + \frac{\partial Q_x}{\partial x} \cdot dx \right] dy - Q_x dy + N_y dx d\theta = 0.$$

[illegible]

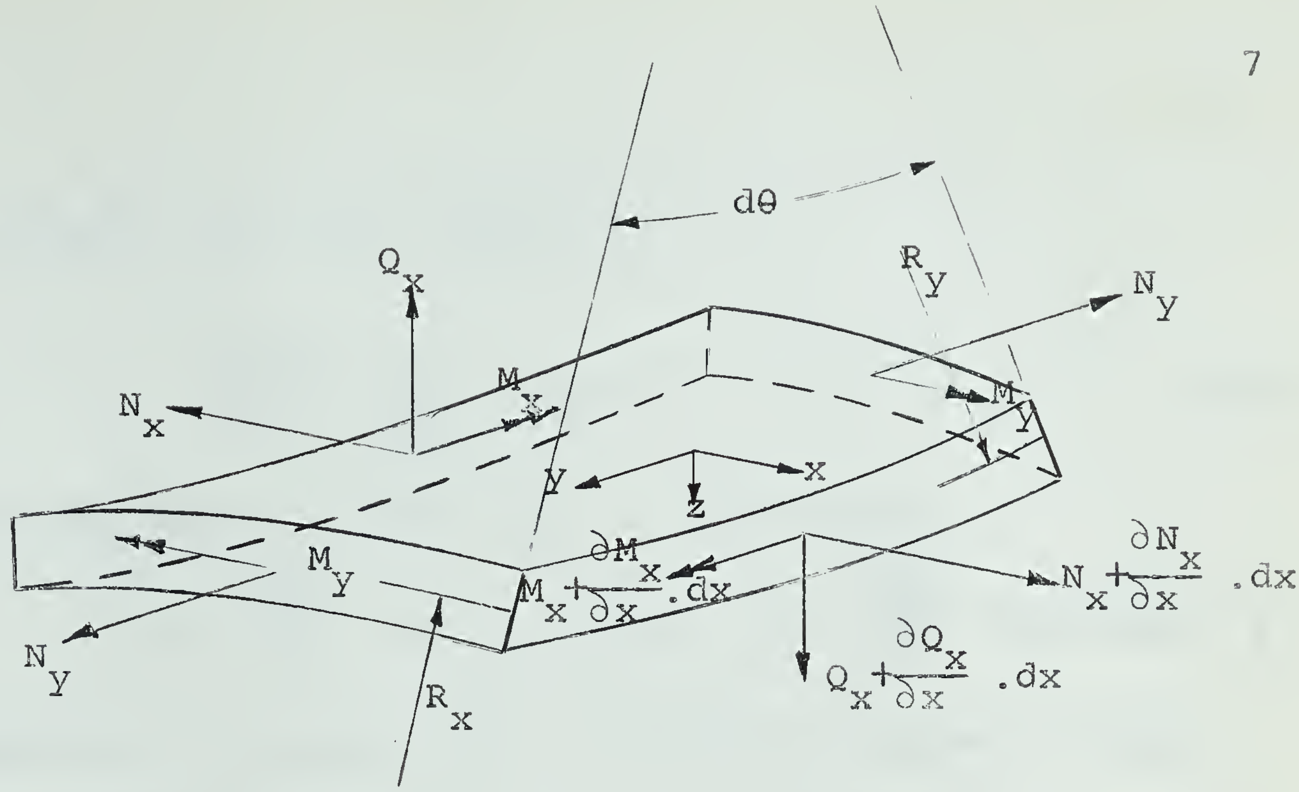

FIGURE 1.1 PLATE ELEMENT

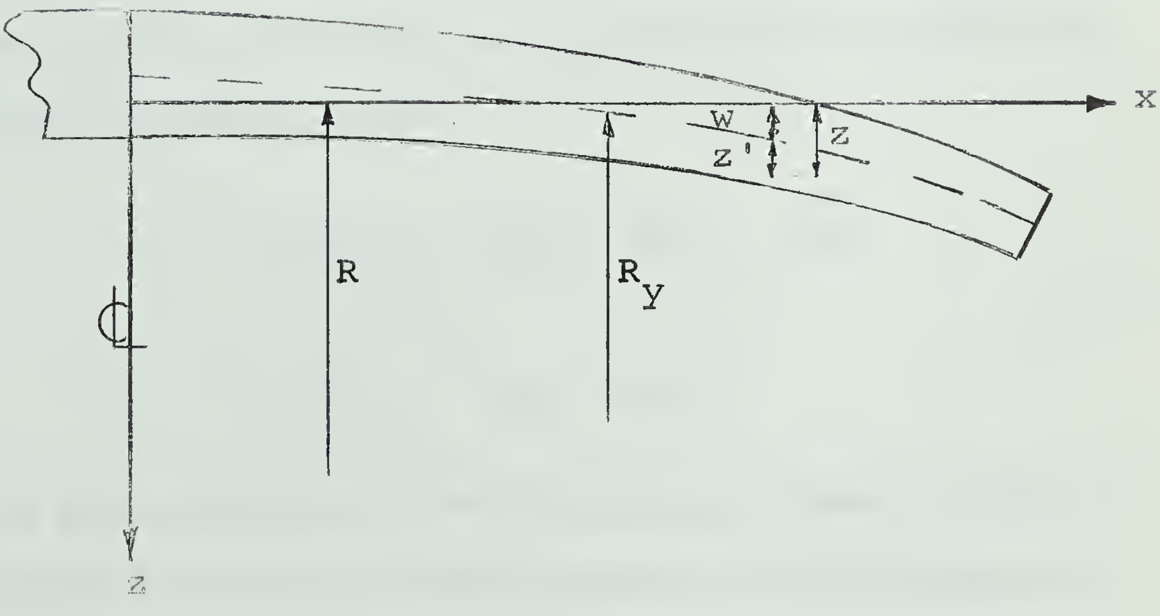

FIGURE 1.2 GEOMETRICAL RELATIONSHIPS

Since $R_y d\theta \doteq dy$ this reduces to

$$\frac{\partial Q_x}{\partial x} + \frac{N_y}{R_y} = 0. \qquad 1.2\text{-}2$$

Moment equilibrium about the y axis gives

$$\left[M_x + \frac{\partial M_x}{\partial x}\ dx\right] dy - M_x dy - \left[Q + \frac{\partial Q_x}{\partial x}\ dx\right] dxdy = 0.$$

Neglecting the second order differential terms as being small compared to the first order the result is

$$\frac{\partial M_x}{\partial x} - Q_x = 0. \qquad 1.2\text{-}3$$

From equations 1.2-2 and 1.2-3 it follows that

$$\frac{\partial^2 M_x}{\partial x^2} + \frac{N_y}{R_y} = 0. \qquad 1.2\text{-}4$$

Hooke's law and the principle of superposition applied to a plane stress problem gives

$$\sigma_x = \frac{E}{(1-\mu^2)} (\epsilon_x + \mu\epsilon_y) \quad \text{and}$$

$$\sigma_y = \frac{E}{(1-\mu^2)} (\epsilon_y + \mu\epsilon_x) . \qquad 1.2\text{-}5$$

Considering the geometrical relationships shown in figure 1.2, the total strain at an arbitrary point in the transverse cross section is

$$\epsilon_y = \frac{-z}{R_y} = \frac{-(z'+w)}{R_y} = \frac{-z'}{R-w} - \frac{w}{R-w} \,. \qquad 1.2\text{-}6$$

Now

$$M_x = \int_{-t/2}^{t/2} z'\sigma_x dz' \,,$$

and using equations 1.2-5 and 1.2-6 this becomes

$$M_x = \frac{-Et^3}{12(1-\mu^2)} \left[\frac{1}{R_x} + \frac{\mu}{R_y} \right]. \qquad 1.2\text{-}7$$

The integration for the moment shows that the first term in equation 1.2-6 is due to bending. The second term is caused by stretching or contracting the middle surface fibers.

The membrane forces induced by this stretching are:

$$N_y = \int_{-t/2}^{t/2} \sigma_y dz' \text{ and } N_x = \int_{-t/2}^{t/2} \sigma_x dz' \,.$$

However N_x equals the stress at the middle surface multiplied by the thickness t therefore

$$N_x = t \left[\sigma_x \right]_{z'=0}$$

but from equation 1.2-1, $N_x = 0$, which gives

$$\left[\epsilon_x + \mu\epsilon_y \right]_{z'=0} = 0. \qquad 1.2\text{-}8$$

Using this result

$$N_y = \int_{-t/2}^{t/2} \sigma_y dz' = E \int_{-t/2}^{t/2} \epsilon_y \Big]_{z'=0} dz' = \frac{-Ewt}{R-w} . \qquad 1.2\text{-}9$$

Substituting equation 1.2-7 and 1.2-9 into equation 1.2-4 the result is

$$\frac{\partial^2}{\partial x^2}\left[- \frac{Et^3}{12(1-\mu^2)} \left(\frac{1}{R_x} + \frac{\mu}{R-w} \right)\right] - \frac{Ewt}{(R-w)^2} = 0.$$

Since the plate is bent with uniformly distributed longitudinal bending moments, each transverse section is subjected to the same loading conditions. It follows that for a given transverse strip w is a function of x only. Therefore, the partial derivatives in the above equation can be replaced by total derivatives.

Also, consider R_x where

$$\frac{1}{R_x} = \frac{\frac{d^2w}{dx^2}}{\left[1 + \left(\frac{dw}{dx}\right)^2\right]^{3/2}}$$

but if $\frac{dw}{dx} \ll 1$ then

$$\frac{1}{R_x} \doteq \frac{d^2w}{dx^2} .$$

The resulting equation is

$$\frac{d^2}{dx^2}\left\{\frac{Et^3}{12(1-\mu^2)}\left[\frac{d^2w}{dx^2}+\frac{\mu}{R-w}\right]\right\}+\frac{Ewt}{(R-w)^2}=0.$$

Since it is assumed that $R-w \doteq R$ simplification of the above gives

$$\frac{d^2}{dx^2}\left(t^3\ \frac{d^2w}{dx^2}\right)+\frac{\mu}{R}\ \frac{d^2}{dx^2}\left(t^3\right)+\ \frac{12(1-u^2)}{R^2}\ wt = 0. \qquad 1.2\text{-}10$$

Lamb[1] solved this equation by considering the transverse section to be of constant thickness.

1.2-2 Extension for Transverse Thickness Variation.

Fung and Wittrick[7] obtained the same result as Lamb[2] using the large deflection equations of von Karman. The authors[7] considered cases where the thickness varied along the cross section and the initial shape of the midline was distorted.

Let $w = \zeta + w_o$ where w_o is the initial distortion of the midline of the cross section measured from the centroidal axis. The additional deflection due to the applied moments is ζ. Considering w_o as a linear function of x, equation 1.2-10 becomes

$$\frac{d^2}{dx^2}\left(t^3\ \frac{d^2\zeta}{dx^2}\right)+\frac{\mu}{R}\ \frac{d^2(t^3)}{dx^2}+\frac{12(1-\mu^2)}{R^2}\ (\zeta+w_o) = 0.$$

Consider a general bi-trapezoidal section shown in figure 1.3.

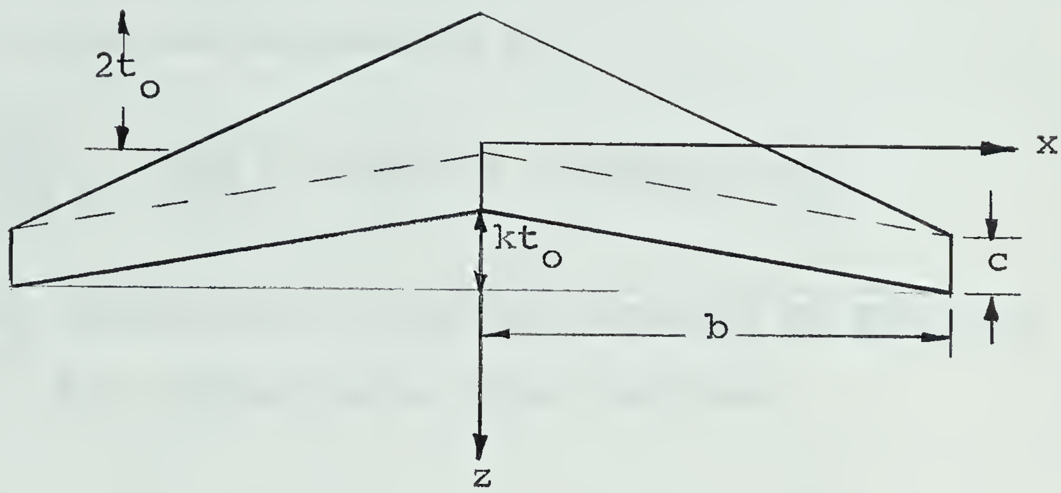

FIGURE 1.3   TRANSVERSE CROSS SECTION

The thickness t, as a function of x, is given by

$$t = 2t_o(1 - \frac{x}{b}) + C \qquad 1.2\text{-}11$$

for any positive x. If the edge thickness c approaches zero the result is the double-wedge shape considered by Fung and Wittrick[7]. If k and t_o are both zero the cross section becomes rectangular.

Equation 1.2-10 can be transformed into non-dimensional terms by setting $\rho = t/t_o$ and $\xi = 1 - x/b$ yielding

$$\frac{d^2}{d\xi^2}\left(\rho^3 \frac{d^2\zeta}{d\xi^2}\right) + \frac{\mu}{R} b^2 \frac{d^2}{d\xi^2}(\rho^3) + 4\lambda^4\rho\,(\zeta + w_o) = 0 \qquad 1.2\text{-}12$$

where $$\lambda^4 = \frac{3(1-\mu^2)b^4}{R^2 t_o^{\,2}} .$$

By making the additional substitutions $\beta = c/2t_o$ and $\gamma = \xi + \beta$, the thickness ratio is given by $\rho = 2\gamma$, and equation 1.2-12 can be reduced to

$$\frac{d^2}{d\gamma^2}\left(\gamma^3 \frac{d^2\zeta}{d\gamma^2}\right) + \frac{6\mu b^2\gamma}{R} + \lambda^4\gamma(\zeta + w_o) = 0. \qquad 1.2\text{-}13$$

This is the differential equation obtained by Fung and Wittrick[7] for double-wedge cross sections.

1.2-3 General Solution of the Differential Equation.

Let ζ_o be the particular integral of equation 1.2-13 so that

$$\frac{d^2}{d\gamma^2}\left(\gamma^3 \frac{d^2\zeta_o}{d\gamma^2}\right) + \lambda^4\gamma\zeta_o = -\lambda^4\gamma w_o - \frac{6\mu b^2}{R}\gamma. \qquad 1.2\text{-}14$$

This gives

$$\zeta_o = -w_o - \frac{6\mu b^2}{\lambda^4 R} \qquad 1.2\text{-}15$$

The total solution is

$$\zeta = \zeta^* + \zeta_o$$

where ζ^* is the complimentary function. Equation 1.2-13 then becomes

$$\frac{d^2}{d\gamma^2}\left(\gamma^3 \frac{d^2\zeta^*}{d\gamma^2}\right) + \lambda^4\gamma\zeta^* = 0$$

and division by γ results in

$$\frac{1}{\gamma}\frac{d^2}{d\gamma^2}\left(\gamma^3 \frac{d^2\zeta^*}{d\gamma^2}\right) + \lambda^4\zeta^* = 0. \qquad 1.2\text{-}16$$

The solution of this equation has been given by Timoshenko[9] and Flugge[10]. Equation 1.2-16 can be reduced to that of two equations of the second order by use of the following identity.

$$\frac{1}{\gamma}\frac{d^2}{d\gamma^2}\left(\gamma^3 \frac{d^2\zeta^*}{d\gamma^2}\right) = \frac{1}{\gamma}\frac{d}{d\gamma}\left\{\gamma^2 \frac{d}{d\gamma}\left[\frac{1}{\gamma}\frac{d}{d\gamma}\left(\gamma^2 \frac{d\zeta^*}{d\gamma}\right)\right]\right\}.$$

Letting $L(\zeta^*) = \frac{1}{\gamma}\frac{d}{d\gamma}\left(\gamma^2 \frac{d\zeta^*}{d\gamma}\right)$,

equation 1.2-16 reduces to

$$L\left[L(\zeta^*)\right] + \lambda^4\zeta^* = 0. \qquad 1.2\text{-}17$$

This equation can be written in one of the following forms.

$$L\left(L(\zeta^*) + i\lambda^2\zeta^*\right) - i\lambda^2\left(L(\zeta^*) + i\lambda^2\zeta^*\right) = 0$$

$$L\left(L(\zeta^*) - i\lambda^2\zeta^*\right) + i\lambda^2\left(L(\zeta^*) - i\lambda^2\zeta^*\right) = 0$$

where $i = \sqrt{-1}$.

Thus, the solutions of the second order equations

$$L(\zeta^*) \pm i\lambda^2\zeta^* = 0 \qquad 1.2\text{-}18$$

must be solutions of 1.2-17. Since these equations have an imaginary coefficient, the solutions are complex-valued functions of γ, and the solutions of one equation will be

the complex conjugates of the other.

Since the solutions are complex conjugates it follows that they are linearly independent of one another. Hence, the two independent solutions of either equation 1.2-18 together will form a complete system of four independent solutions. Assume

$$\zeta_1^* = \theta_1 + i\theta_2$$

$$\zeta_2^* = \theta_3 + i\theta_4$$

are two independent solutions of

$$L(\zeta^*) + i\lambda^2\zeta^* = 0$$

then

$$\zeta_3^* = \theta_1 - i\theta_2$$

$$\zeta_4^* = \theta_3 - i\theta_4$$

are solutions of

$$L(\zeta^*) - i\lambda^2\zeta^* = 0.$$

All four solutions represent the complete system of independent solutions. By using sums and differences of these solutions the general solution of 1.2-17 can be represented as

$$\zeta^* = C_1\theta_1 + C_2\theta_2 + C_3\theta_3 + C_4\theta_4.$$

To determine the functions θ, solution of only one of the

second order equations above is needed. Consider

$$L(\zeta^*) + i\lambda^2\zeta^* = 0.$$

Writing the differential operator in full we obtain

$$\gamma \frac{d^2\zeta^*}{d\gamma^2} + 2 \frac{d\zeta^*}{d\gamma} + i\lambda^2\zeta^* = 0.$$

Now set $\psi = 2\lambda(i\gamma)^{1/2} = \eta\sqrt{i}$ and $v = \zeta^*\sqrt{\gamma}$

then we obtain

$$\psi^2 \frac{d^2v}{d\psi^2} + \psi \frac{dv}{d\psi} + (\psi^2-1)v = 0.$$

The solutions of this equation are the Bessel functions of the first order of the complex argument ψ giving

$$v = AJ_1(\psi) + B\,H_1(\psi).$$

The Bessel functions $J_1(\psi)$, $H_1(\psi)$ of the first order, are connected to the zero order functions by

$$J_1(\psi) = \frac{-d}{d\psi} Jo(\psi), \qquad H_1(\psi) = \frac{-d}{d\psi} Ho(\psi)$$

The real and imaginary parts of Jo and Ho may be considered as real functions of the real variable η. These functions are known as Thomson or Kelvin functions(11).

The Thomson functions are introduced by the following formulae

$$Jo(\psi) = Jo(\eta\sqrt{i}) = \mathrm{ber}\,\eta - i\,\mathrm{bei}\,\eta$$

$$Ho(\psi) = Ho(\eta\sqrt{i}) = \frac{-2}{\pi}(\mathrm{kei}\,\eta + i\,\mathrm{ker}\,\eta)$$

[illegible]

$$[illegible]$$

[illegible]

$$[illegible]$$

[illegible]

[illegible]

$$[illegible]$$

[illegible]

[illegible]

$$[illegible]$$

[illegible]

[illegible]

$$[illegible]$$

[illegible]

[illegible]

[illegible]

[illegible]

[illegible]

[illegible]

[illegible]

[illegible]

Differentiating with respect to ψ and separating real and imaginary parts, a set of relations for the first order functions are obtained,

$$J_1(\psi) = \frac{1}{\sqrt{2}} \left[(\mathrm{bei}'\eta - \mathrm{ber}'\eta) + i(\mathrm{bei}'\eta + \mathrm{ber}'\eta)\right]$$

$$H_1(\psi) = \frac{\sqrt{2}}{\pi} \left[(\mathrm{ker}'\eta + \mathrm{kei}'\eta) + i(\mathrm{ker}'\eta - \mathrm{kei}'\eta)\right] ,$$

where the prime denotes differentiation with respect to η.

The solution of equation 1.2-16 can be written as

$$\zeta^* = \frac{1}{\eta} \left[S\ \mathrm{ber}'\eta + T\ \mathrm{bei}'\eta + U\ \mathrm{ker}'\eta + V\ \mathrm{kei}'\eta\right] ,$$

and the complete solution of equation 1.2-13 becomes

$$\zeta = \frac{1}{\eta} \left[S\ \mathrm{ber}'\eta + T\ \mathrm{bei}'\eta + U\ \mathrm{ker}'\eta + V\ \mathrm{kei}'\eta\right] - w_o - \frac{6\mu b^2}{\lambda^4 R} \qquad 1.2\text{-}19$$

1.2-4 Constants of Integration

At the free edge ($x = b$) the boundary conditions show that the moments and shear forces on a plane whose normal is in the x direction are zero giving

$$M_x = \frac{-Et^3}{12(1 - \mu^2)} \left[\frac{d^2w}{dx^2} + \frac{\mu}{Ry}\right]_{x=b} = 0 \quad \text{and}$$

$$V_x = \left[Q_x + \frac{\partial}{\partial y} (M_{xy})\right]_{x=b} = 0 .$$

Since $M_{xy} = 0$ the condition that $V_x = 0$ reduces to

$$\left[\frac{d^3w}{dx^3}\right]_{x=b} = 0.$$

Transformed to non-dimensional terms this becomes

$$\left[\frac{d^3\zeta}{d\eta^3} - \frac{3}{\eta}\frac{d^2\zeta}{d\eta^2} + \frac{3}{\eta^2}\frac{d\zeta}{d\eta}\right]_{\eta=2\lambda\beta^{1/2}} = 0. \qquad 1.2\text{-}20$$

The condition $M_x = 0$ at the free edge results in

$$\left[\frac{d^2w}{dx^2}\right]_{x=b} = \frac{-\mu}{R}$$

where $\qquad R_y = R - w \doteq R$

and transforming this to non-dimensional terms gives

$$\left[\frac{d^2\zeta}{d\eta^2} - \frac{1}{\eta}\frac{d\zeta}{d\eta}\right]_{\eta=2\lambda\beta^{1/2}} = \left[-\frac{\mu b^2}{4\lambda^4 R}\eta^2\right]_{\eta 2\lambda\beta^{1/2}} . \qquad 1.2\text{-}21$$

The symmetry of the problem allows the condition $\left[\frac{d\zeta}{dx}\right]_{x=0} = 0.$

In non-dimensional terms this is

$$\left[\frac{d\zeta}{d\eta}\right]_{n=2\lambda(1+\beta)^{1/2}} = 0. \qquad 1.2\text{-}22$$

The fourth condition results from the boundary condition

$$\int_{-b}^{b} N_y d_x = 0 ,$$

and can be simplified with equation 1.2-9 giving

$$\int_0^b (w_o + \zeta)\ t dx = 0.$$

Since the problem is symmetrical about the longitudinal axis, this integral is written for only half the transverse cross section. The transformation of the above equation to non-dimensional terms gives

$$\int_\beta^{1+\beta} \zeta\gamma d\gamma = 0. \qquad 1.2\text{-}23$$

Before evaluating equations 1.2-20 to 1.2-23 w_o must be determined. For the section considered in figure 1.3, w_o is given by

$$w_o = -t_o(1+k)\gamma + t_o\ (1+k)\ \frac{(2\beta^2 + 2\beta + 2/3)}{(2\beta + 1)}$$

The four conditions given by equations 1.2-20 to 1.2-23 result in four equations for the constants S,T,U and V. These are given below where, for simplification,

$$\alpha = 2\lambda(1+\beta)^{1/2} \qquad \epsilon = 2\lambda\beta^{1/2}$$

$$\begin{aligned}0 = {} & S\left[-\epsilon^3 \text{ ber } \epsilon - 24\epsilon \text{ bei } \epsilon - 48 \text{ ber}'\epsilon + 8\epsilon^2 \text{ bei}'\epsilon\right] \\ & + T\left[-\epsilon^3 \text{ bei } \epsilon + 24\epsilon \text{ ber } \epsilon - 48 \text{ bei}'\epsilon - 8\epsilon^2 \text{ ber}'\epsilon\right] \\ & + U\left[-\epsilon^3 \text{ ker } \epsilon - 24\epsilon \text{ kei } \epsilon - 48 \text{ ker}'\epsilon + 8\epsilon^2 \text{ kei}'\epsilon\right] \\ & + V\left[-\epsilon^2 \text{ kei } \epsilon + 24\epsilon \text{ ker } \epsilon - 48 \text{ kei}'\epsilon - 8\epsilon^2 \text{ ker}'\epsilon\right]\end{aligned} \qquad 1.2\text{-}20a$$

[illegible]

[illegible]

[illegible]

[illegible]

[illegible]

[illegible]

[illegible]

$$0 = S\left[4\epsilon \text{ bei } \epsilon - \epsilon^2 \text{ bei}'\epsilon + 8 \text{ ber}'\epsilon\right]$$

$$+ T\left[-4\epsilon \text{ ber } \epsilon + \epsilon^2 \text{ ber}'\epsilon + 8 \text{ ber}'\epsilon\right]$$

$$+ U\left[4\epsilon \text{ kei } \epsilon - \epsilon^2 \text{ kei}'\epsilon + 8 \text{ ker}'\epsilon\right]$$

$$+ V\left[-4\epsilon \text{ ker } \epsilon + \epsilon^2 \text{ker}'\epsilon + 8 \text{ kei}'\epsilon\right] + \frac{\mu b^2 \beta \epsilon^3}{R\lambda^2} \qquad 1.2\text{-}21a$$

$$0 = S\left[-\alpha \text{bei } \alpha - 2 \text{ ber}'\alpha\right] + T\left[\alpha \text{ ber } \alpha - 2 \text{ bei}'\alpha\right]$$

$$+ U\left[-\alpha \text{kei } \alpha - 2 \text{ ker}'\alpha\right] + V\left[\alpha \text{ ker } \alpha - 2 \text{ kei}'\alpha\right]$$

$$+ \frac{t_o \alpha^3 (1+k)}{2\lambda^2} \qquad 1.2\text{-}22a$$

$$0 = S\left[\alpha^2 \text{ ber } \alpha - 2\alpha \text{ bei}'\alpha - \epsilon^2 \text{ ber } \epsilon + 2\epsilon \text{ bei}'\epsilon\right]$$

$$+ T\left[\alpha^2 \text{ bei } \alpha + 2\alpha \text{ ber}'\alpha - \epsilon^2 \text{ bei } \epsilon - 2\epsilon \text{ ber}'\epsilon\right]$$

$$+ U\left[\alpha^2 \text{ ker } \alpha - 2\alpha \text{kei}' \alpha - \epsilon^2 \text{ ker } \epsilon + 2\epsilon \text{ kei}'\epsilon\right]$$

$$+ V\left[\alpha^2 \text{ kei } \alpha + 2\alpha \text{ker}' \alpha - \epsilon^2 \text{ kei } \epsilon - 2\epsilon \text{ ker}'\epsilon\right]$$

$$- \frac{6\mu b^2}{\lambda^4 R} \; \frac{(\alpha^4 - \epsilon^4)}{4} \qquad 1.2\text{-}23a$$

The solution of the above equations for the constants in the general solution was obtained using an IBM 7040/1401 digital computer. Details of this solution appear in Appendix I.

[illegible]

$$[illegible]$$

[illegible] $$[illegible]$$

$$[illegible]$$

[illegible] $$[illegible]$$

[illegible] $$[illegible]$$

[illegible]

<u>1.3 Comparison of Results to Previous Work.</u>

Earlier investigators showed solutions for a uniform plate and for a tapered plate with a line edge. Bellow[12] gave the results of Lamb's solution for a uniform plate. Fung and Wittrick[7] gave results for the linearly tapered plate with a line edge. By changing parameters in the above solution, both of these earlier results can be closely approximated.

Using the theory developed above, neither the flat plate nor the tapered plate with line edge solution can be reached exactly. For the uniform plate, the thickness of the tapered portion, $2t_o$, must be zero. This would cause the value of λ to become infinite. The tapered plate with the free edges being lines is obtained when the edge thickness c goes to zero. With c zero, the variable η is zero at the free edges and the ker' function becomes negative infinity. For this case of zero edge thickness, the boundary conditions of zero moment and zero shear along the free edges no longer have any meaning. Even though these solutions can not be reached exactly they can be closely approximated by giving t_o and c values which are small compared to the total thickness of the plate.

In figure 1.4 the deflections of a uniform plate are compared to those using the theory developed above. These curves were obtained for a value of t_o which was approxi-

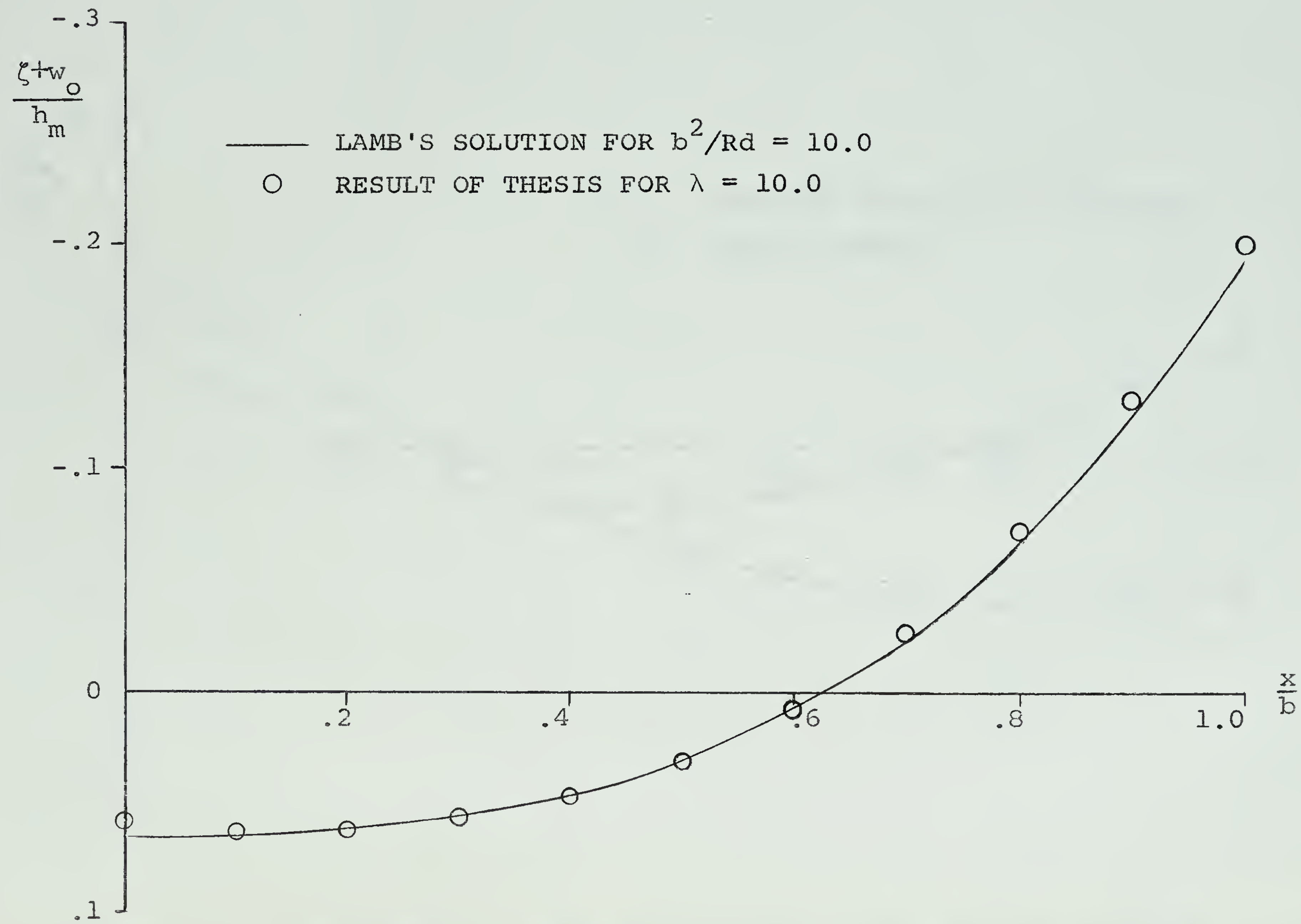

FIGURE 1.4 COMPARISON OF THEORETICAL RESULT WITH LAMB'S SOLUTION

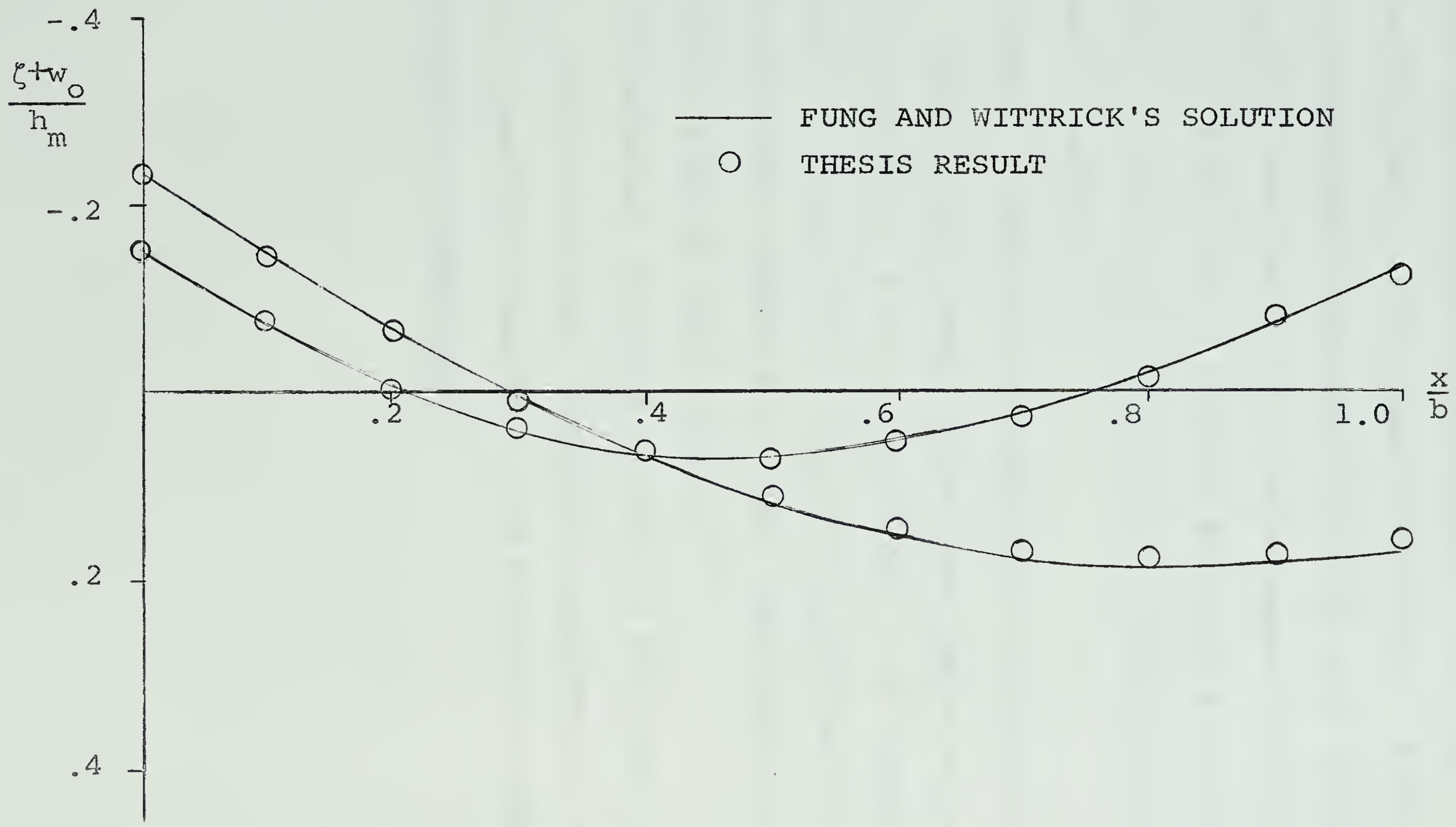

FIGURE 1.5 COMPARISON OF THEORETICAL RESULT WITH FUNG AND WITTRICK'S SOLUTION

mately 4 percent of the total thickness. The curves are compared on the basis of the same b^2/Rt ratio. Actual flat plate results were obtained from work done by Bellow[12] since these were available for a large range of b^2/Rt ratios. It must be noted that the b used by Bellow was the total plate width, not half the width as used in the theoretical development of section 1.2.

Figure 1.5 shows the comparison to Fung and Wittrick's[7] results. Their results were taken from graphs so the reproduction in figure 1.5 may not be exact. To compare with these results a solution for c equal to approximately 4 percent of the maximum thickness is used. The definition of λ is the same as used by these authors [7].

The agreement obtained in each of the above cases is good. In the following chapters, experimental verification, for specific cases which lie between the extremities discussed above, is undertaken.

CHAPTER II

EXPERIMENTAL CONSIDERATIONS

2.1 Numerical Integration Technique

The curvature in the transverse direction due to the distortion of the midline is

$$\frac{1}{R_x} = \frac{d^2\zeta}{dx^2}$$

when using the assumption that the square of the slope, $\left(\frac{d\zeta}{dx}\right)^2$ is small compared to unity. Double integration of this expression with respect to x, the coordinate in the transverse direction, results in

$$\zeta(x) = \int_{c_1}^{x} \int_{c_2}^{x} \frac{d^2\zeta}{dx^2}\, dxdx$$

where c_1 and c_2 are arbitrary constants.

Consider a transverse strip with curvature $1/R_{x_i}$ at the point x_i. Let the strains indicated by the two strain gauges mounted on the upper and lower surfaces of this plate at the point x_i be e_{T_i} and e_{B_i}, respectively. The bending strain at a point in a fiber is known to be directly proportional to the curvature at that point by the relation

$$e = -\frac{z}{R_x}$$

[illegible]

[illegible]

[illegible]
[illegible]
[illegible]

$$[illegible]$$

[illegible]
[illegible]
[illegible]
[illegible]

$$[illegible]$$

[illegible]
[illegible]
[illegible]
[illegible]
[illegible]
[illegible]
[illegible]
[illegible]

[illegible]

where z is the distance from the neutral surface to the point. Considering the upper surface of the plate, the bending strain becomes

$$(e_{bending})_i = \frac{t_i}{2R_{x_i}} \tag{2.2-1}$$

where t_i is the thickness of the strip at x_i.

Since the actual measured strains may include membrane strains these must be subtracted. The membrane strain is given by the average value of e_{T_i} and e_{B_i} with the resulting bending strain

$$(e_{bending})_i = e_{T_i} - \frac{(e_{T_i} + e_{B_i})}{2} = \frac{e_{T_i} - e_{B_i}}{2}$$

and the curvature is then given by

$$\frac{1}{R_{x_i}} = \frac{e_{T_i} - e_{B_i}}{t_i} \tag{2.2-2}$$

To calculate the deflections from the curvatures required a double integration which was done numerically. The trapezoidal rule[13] which was used in this process has been described by Bellow et al [3]. The first integration results in the slope of the distortion curve. This distortion curve is symmetrical about the center of the transverse section so the integration was started at the point x = 0 where

$$\left[\frac{d\zeta}{dx}\right]_{x=0} = 0.$$

The second integration, which gave the distortion of the midline of the section, was also started at the plate center. The distortion of the midline, was calculated relative to the center of the cross section ($x = 0$). To comply with the boundary conditions in Chapter I the distortion was to be measured relative to the centroidal axis, so the trapezoidal rule was used again to calculate the position of the centroid.

If the distance between two neighbouring measuring stations is $h = x_{i+1} - x_i$ then the length of the line joining the points representing the distortion at x_i and x_{i+1} is

$$\left[h^2 + \left(\zeta_{i+1} - \zeta_i\right)^2\right]^{1/2}$$

The first moment of area of this portion of the cross section (between x_i and x_{i+1}) about the horizontal axis through

$$\left[\zeta\right]_{x=0} = 0$$

is

$$\left(\frac{\zeta_i + \zeta_{i+1}}{2}\right)\left(\frac{t_i + t_{i+1}}{2}\right)\left[h^2 + \left(\zeta_{i+1}-\zeta_i\right)^2\right]^{1/2} . \quad 2.2\text{-}3$$

Multiplying equation 2.2-3 by h/h the result is

$$h\left(\frac{\zeta_i + \zeta_{i+1}}{2}\right)\left(\frac{t_i + t_{i+1}}{2}\right)\left[1 + \left(\frac{\zeta_{i+1} - \zeta_i}{h}\right)^2\right]^{1/2} .$$

Assuming again that the square of slope of the distortion curve is small compared to unity, the last term in the above is negligible. The moment of this segment of the cross section reduces to

$$h\left(\frac{\zeta_i + \zeta_{i+1}}{2}\right)\left(\frac{t_i + t_{i+1}}{2}\right) .$$

The centroid of the distorted curve is given by

$$\bar{\zeta}A = \int_{-b}^{b} \zeta t dx$$

where A is the area of the cross section. Therefore, $\bar{\zeta}$ is

$$\bar{\zeta} = \frac{h}{4A}\left[\left(\zeta_o + \zeta_1\right)\left(t_o + t_1\right) + \ldots + \left(\zeta_{n-1} + \zeta_n\right)\left(t_{n-1} + t_n\right)\right] \qquad 2.2\text{-}4$$

where n is the number of measuring stations. The more measuring stations used the closer the above analysis approaches the actual case. The distortion of the midline is given by $\zeta_{True} = \zeta - \bar{\zeta}$ and the position of the midline of the cross section is given by

$$w = \zeta_{True} + w_o \qquad 2.2\text{-}5$$

The initial deflection of the midline of the cross section, w_o, is given relative to the centroidal axis.

[illegible]

[illegible]
[illegible]
[illegible]
[illegible]

[illegible]

[illegible]

[illegible]

[illegible]
[illegible]

[illegible]

[illegible]
[illegible]
[illegible]
[illegible]
[illegible]

[illegible]

[illegible]
[illegible]

2.2 Experimental Apparatus

2.2-1 Plates

The plates tested were machined from a flat rolled sheet of Alclad 7075-T6*. This material has a modulus of elasticity of 10.4×10^6 psi and a Poisson's ratio of 0.333 and was chosen because it had a higher yield stress and a lower modulus of elasticity than mild steel. The high yield stress allowed larger longitudinal curvatures than possible with mild steel. With a lower modulus of elasticity than steel a specific curvature could be obtained with a smaller load.

The first plate tested, Plate I, was machined from a sheet of aluminum 0.125 x 12.0 x 67.0 inches. The bi-trapezoidal cross section was obtained using an end-mill cutter on a vertical milling machine. Figure 2.1 shows half the transverse cross section of the finished plate and the cross section as it was assumed to be for calculation purposes. During the machining a warping of the entire cross section occurred (the bottom edge was initially flat), with pronounced curling at the edges. The cross

---

* Designation and properties of the alloy used were obtained from Alcoa Structural Handbook, Aluminum Company of American, 1956, p35.

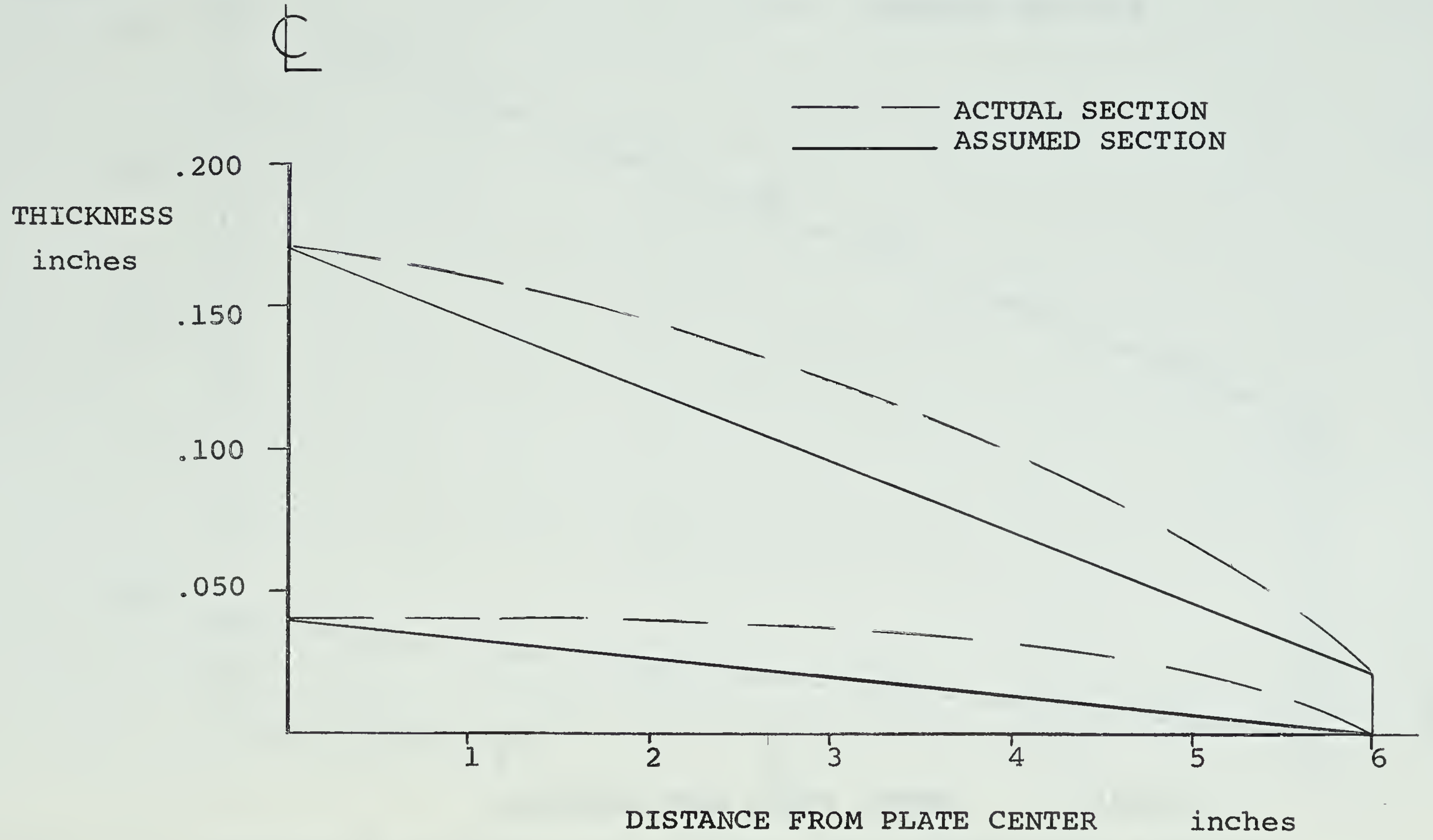

FIGURE 2.1 COMPARISON OF ACTUAL AND ASSUMED CROSS SECTION FOR PLATE I

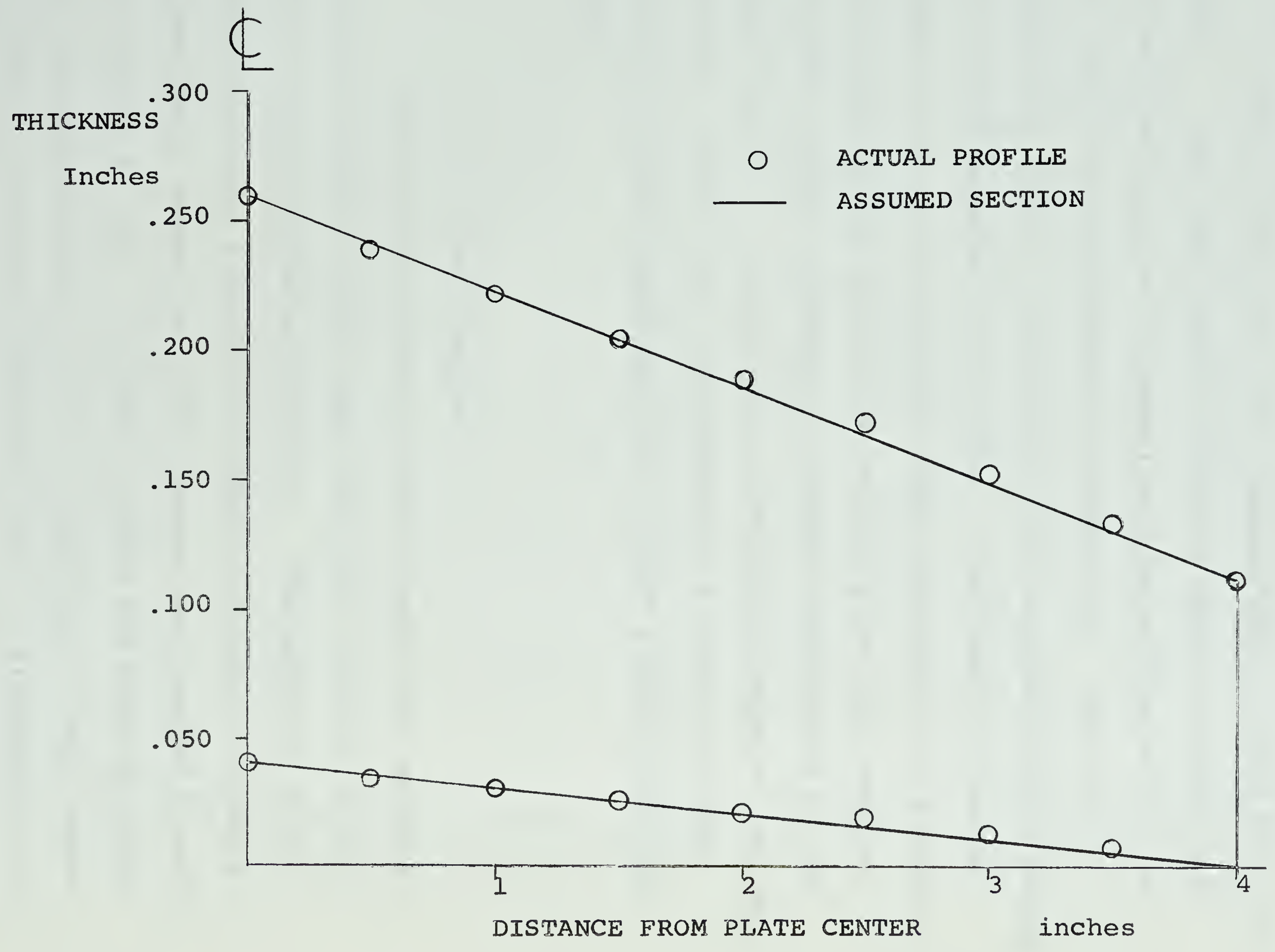

FIGURE 2.2. COMPARISON OF ACTUAL AND ASSUMED CROSS SECTION FOR PLATE II

section dimensions were chosen so that λ could be varied over the range $0 < \lambda < 7.5$.

Plate II was cut from aluminum sheet 0.25 x 8.0 x 70.0 inches. The final section, which is shown in figure 2.2 was obtained using a horizontal milling machine with a 4-inch long, 2.5-inch diameter cutting tool. This tool allowed one side of the section to be machined without moving the tool transverse to the plate. The result, shown in figure 2.2 shows the straight edges obtained by this method. The section warped during the machining but this warping was quite linear, allowing an accurate description of the actual section. As a result of the final shape of the cross section, λ values up to approximately 4.0 were all that could be obtained experimentally without yielding the material.

2.2-2 Strain Gauges

Electrical resistance strain gauges were mounted along the midline on the upper and lower surfaces of the plate in the transverse direction. The position of the gauges on Plates I and II are shown in figures 2.3 and 2.4, respectively, where the bottom gauges were mounted directly below those on top. In order to keep the error in using the trapezoidal rule as small as possible, a large number of measuring stations should be used. A discussion of the

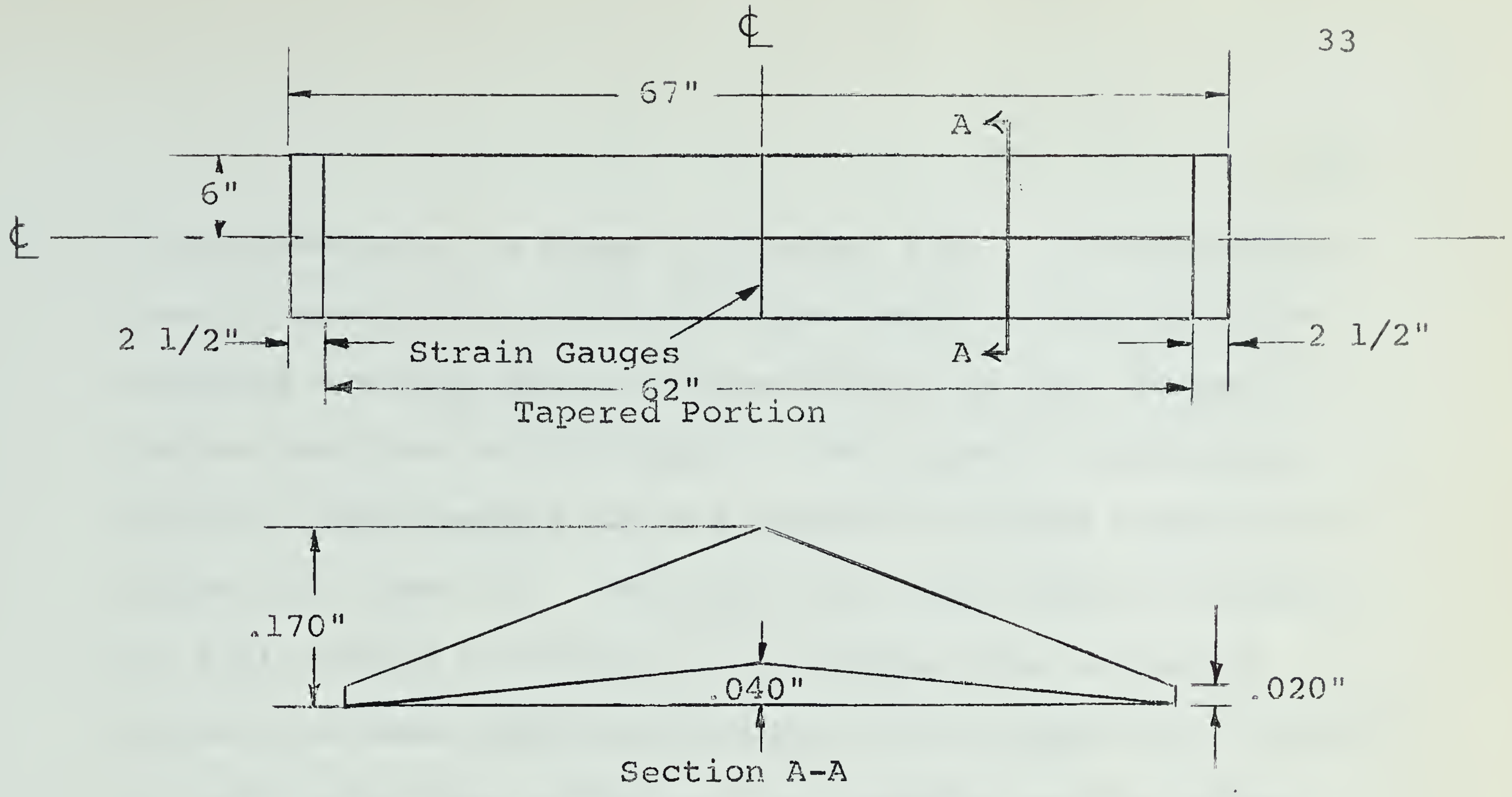

FIGURE 2.3 PLATE I

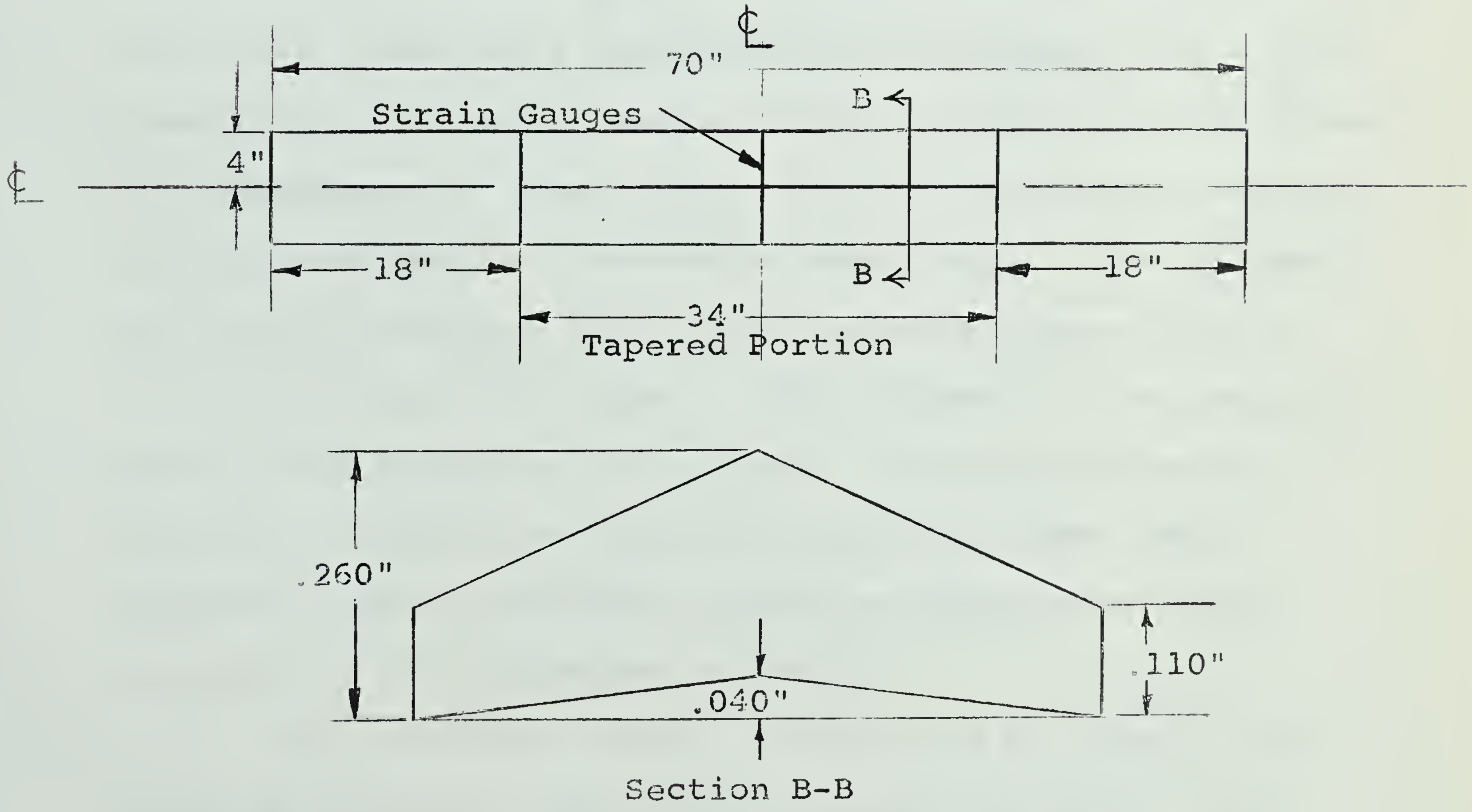

FIGURE 2.4 PLATE II

truncation error is given in Chapter III. It was decided that 13 stations on half the cross section would give the required accuracy while the application of this number of gauges would not be difficult. As a result the distance between gauge centers was 0.5 inches for Plate I and 0.333 inches for Plate II. To obtain the gauge center distance of 0.333 inches for Plate II the gauges were staggered. As well as these transverse gauges, four longitudinal gauges on each plate (two on top and two opposite on the bottom) were used to calculate the longitudinal curvature.

The strain gauges used were "Budd" metal film electrical resistance gauges type C12-121. These gauges, which are temperature compensated for aluminum, have a grid length of 0.125 inches and an overall length of 0.250 inches. Two advantages of these gauges are the thin backing material on the gauge and low transverse sensitivity. The thinner the backing material the closer the actual gauge grid is to the surface of the plate. This allows a closer measurement of the strain at the surface. Low transverse sensitivity is important since the plate was under large strains in the longitudinal direction compared to those measured in the transverse direction.

To obtain the strains as close to the edge of the plate as possible, type C12-111 gauges were used. These have a grid length of 0.063 inches with the result that the

gauge center was 0.0315 inches from the edge. Since the distance between gauges was assumed to be constant the small error introduced was assumed to be negligible in the analysis.

2.2-3 Loading Apparatus

The method of applying a uniformly distributed moment to the longitudinal ends of the plate was similar to that used by Conway and Nickola[4]. The two ends of the test plate were bolted on one-inch diameter shafts. These shafts were keyed to pulleys, and loading of the plates was done by applying loads to the rims of these pulleys. This loading system, which was supported on bearings to reduce the frictional effects, is shown in figure 2.5.

The loading arrangements discussed above had the advantage of being adaptable to different length and width of plates. Pulley sizes were easily changed allowing reasonable loads to be used in obtaining the desired curvature. A 6-inch diameter pulley was used with Plate I while a 15-inch diameter pulley was used with Plate II.

To check the influence of the support condition on the tapered plate, a second set of transverse strain gauges were mounted on Plate I approximately one foot from one of the edges being loaded. The results of tests with

[illegible]
[illegible]
[illegible]
[illegible]

[illegible]

[illegible]

[illegible]

[illegible]

[illegible]

[illegible]

[illegible]

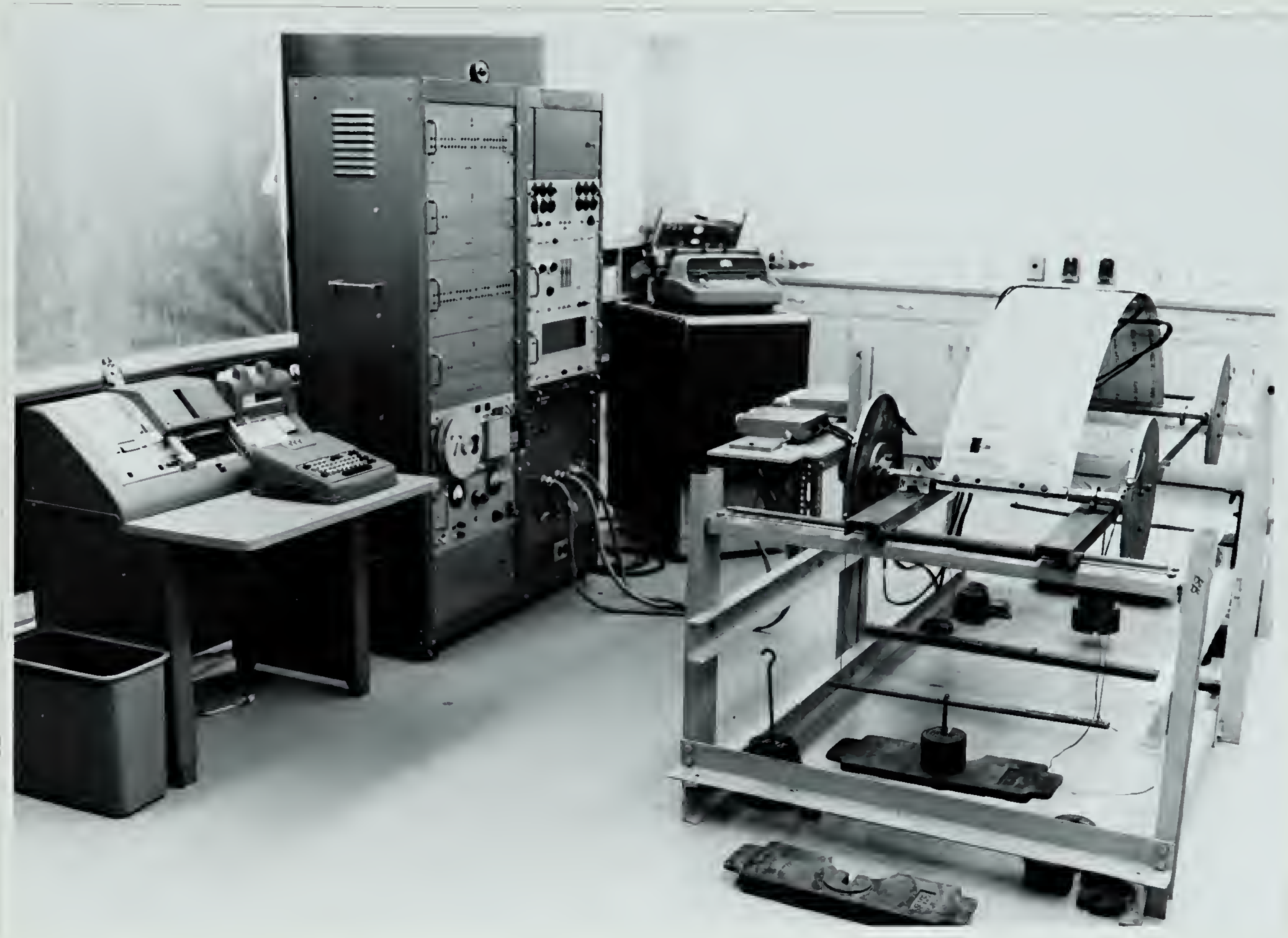

FIGURE 2.5 VIEW OF APPARATUS

these gauges showed little or no difference to those located 2.5 feet from the loaded edges. Other tests were made with the supports each 18 inches from the section being tested. Again, little difference in the results was observed.

2.2-4 Recording and Associated Equipment

A multichannel digital data processor* was used to measure the voltage drop across the strain gauges and convert this analog reading to a digital one. This apparatus was calibrated so that the output was the strain measured in microinches per inch. Recording of the strains was done with an IBM 024 card punch. Since a card punch had not been used in conjunction with the processor previously, a description of the electrical hook-up of the card punch to processor is given in Appendix III. A picture of this system is shown in figure 2.5.

The strains, which were recorded on IBM cards, were used as data for a Fortran IV computer program. This program, which was run on the IBM 7040/1401 system, cal-

---

* Design and operation of this processor has been discussed by Bellow (12).

culated the deflections by the numerical method outlined in section 2.2. Appendix II includes a description of the program used.

2.3 Test Procedure

The procedure for testing both plates was essentially the same. The plate being tested was initially put on a flat surface where the "zero" or initial readings of the strains were taken. Actually the zero balancing system of the processor was used to bring the strains as close to zero as possible. The "zero" readings were then taken. These initial strains were subtracted from those taken under load to obtain the absolute change in strain due to the load. The plate was loaded by adding weights to the loading hangers and thereby applying a uniformly distributed moment to the transverse edges of the plate. At the various λ values the transverse strains were recorded on the card punch. The output of the processor was also printed on a typewriter to give a check on the strain readings. If the readings were abnormal they could be disregarded and another set taken. Once the largest curvature was reached, and the transverse strains recorded, the plate was unloaded. During the unloading the transverse strains were again recorded at the various λ values. After unloading, with the plate again

resting on a flat surface, another set of strains were recorded and these checked against the initial readings to see if the strain gauges were functioning properly.

It was found, that after a loading program, as indicated in the above paragraph, some of the gauges tended to drift. In order to minimize this drift, it was decided to take a set of "zero" strain readings before each load was applied to the plate. These "zero" strains were subtracted from the strains recorded under the load next applied to give an absolute strain reading. More consistent results were obtained by this testing scheme than by the first procedure.

As many as 10 tests were taken at each λ value. The results of these tests are shown in the following chapter.

CHAPTER III

EXPERIMENTAL AND THEORETICAL RESULTS

3.1 Remarks on Experimental Results

Since the plates and the loads applied to them were symmetrical about the longitudinal y-axis, the results of both halves of the transverse cross section were compared to the theoretical curves for half the cross section. In this way two sets of experimental results were obtained from each test. The plates were loaded to produce the longitudinal curvatures corresponding to the various λ values at least 5 and sometimes 10 times each. As a result, there were at least 10 and up to 20 sets of results to compare for each λ value.

Figure 3.1 shows a typical range of values obtained experimentally for Plate I. When scattering of results occurred as shown in figure 3.1, more than the minimum of five tests were taken. The results shown in the following sections for Plate I, are the averages obtained from a series of tests at the particular λ value.

The experimental results of Plate II were more precise than those of Plate I. The graphical representation of these tests showed the points from various tests to be almost indistinguishable from one another. The results of

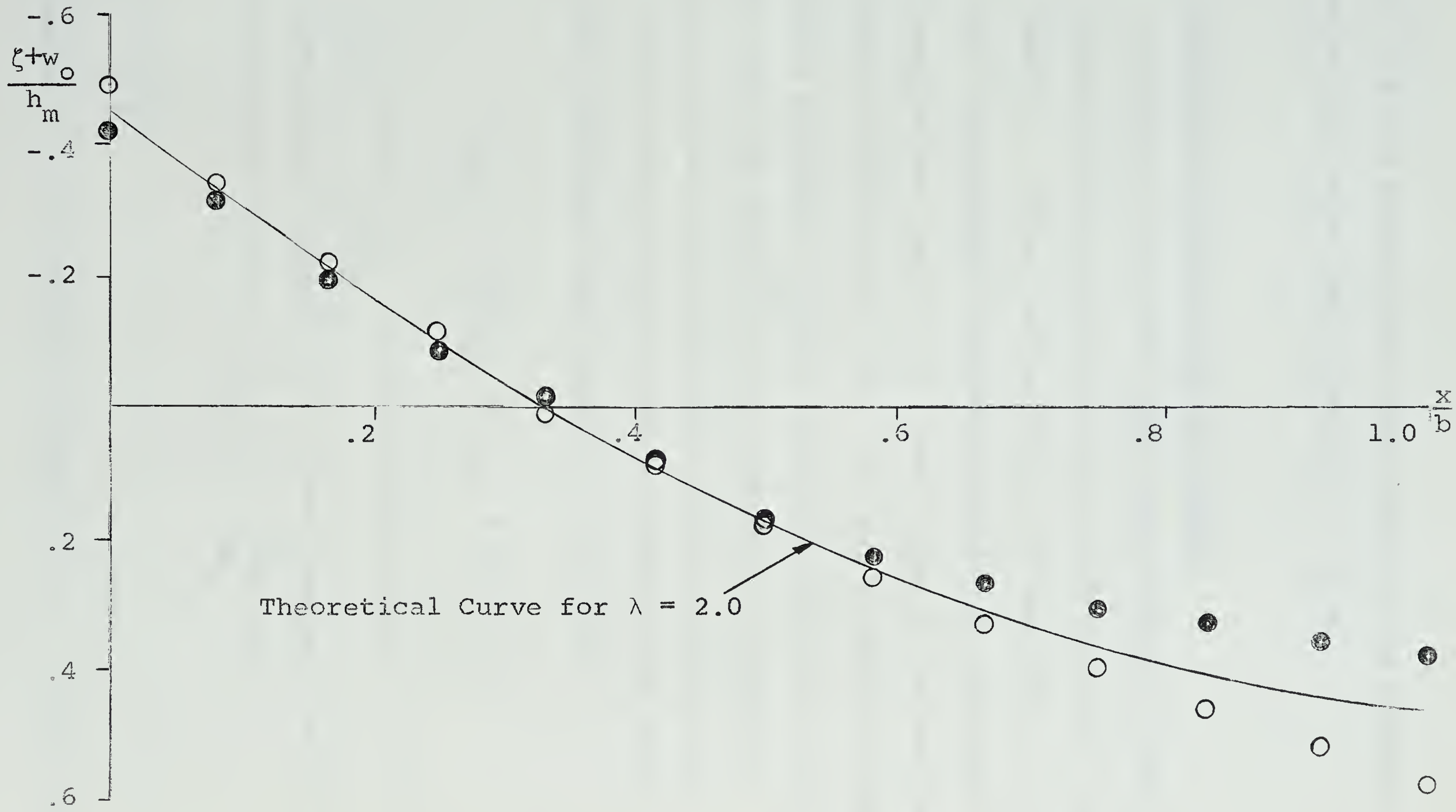

FIGURE 3.1 TYPICAL RANGE OF EXPERIMENTAL RESULTS FOR PLATE I

between five and seven tests were averaged and compared with the theoretical curve for a specific λ value.

3.2 Comparison of Experiment and Theory

Initially it was felt that the warping of the plates, which occurred during the machining, would not affect the final results. After testing Plate I extensively it was found that the agreement between theoretical and experimental results was poor if the lower edge of the section was assumed to be flat ($k = 0$). It was decided to check the bending stresses in the transverse direction to see if there were any errors in the numerical integration technique used to obtain the experimental deflections.

The bending stress in the x-direction at point x_i of the transverse cross section is given by

$$\left(\sigma_{x_B}\right)_i = \frac{E}{(1-\mu^2)} \left[\left(\epsilon_{x_B}\right)_i + \mu\left(\epsilon_{y_B}\right)_i\right] \qquad 3.2\text{-}1$$

where $\left(e_{x_B}\right)_i$ and $\left(e_{y_B}\right)_i$ are the bending strains in the x and y directions, respectively. These bending strains are given by equation 2.2-1 as $\left(e_{x_B}\right)_i = \frac{-t_i}{2R_{x_i}}$ and

$$\left(e_{y_B}\right)_i = \frac{-t_i}{2\,R_y}$$

where again t_i is the plate thickness at x_i. Using the

assumption that

$$\frac{1}{R_x} \doteq \frac{d^2\zeta}{dx^2} \quad ,$$

then

$$\left(e_{x_B}\right)_i = \frac{-t_i}{2}\,\frac{d^2\zeta}{dx^2} \; , \qquad 3.2\text{-}2$$

and since $R - w = R_y \doteq R$

$$\left(e_{y_B}\right)_i = -\frac{t_i}{2R} \; . \qquad 3.2\text{-}3$$

Substituting equations 3.2-2 and 3.2-3 into 3.2-1 the result is

$$\left(\sigma_{x_B}\right)_i = \frac{-Et_i}{2(1-\mu^2)}\left[\frac{d^2\zeta}{dx^2} + \frac{\mu}{R}\right]. \qquad 3.2\text{-}5$$

This formula was used to calculate the transverse bending stress theoretically. The experimental bending stresses were also found using equation 3.2-1. The value of $\left(e_{y_B}\right)_i$ is the same as used in the theoretical result in the above paragraph. The bending strain in the x-direction $\left(e_{x_B}\right)_i$ was found to be

$$\left(e_{x_B}\right)_i = \frac{e_{T_i} - e_{B_i}}{2}$$

in section 2.2. The bending stress $\left(\sigma_{x_B}\right)_i$ from the experiment was then calculated from

$$\left(\sigma_{x_B}\right)_i = \frac{E}{2(1-\mu)^2}\left[e_{T_i} - e_{B_i} - \frac{\mu t_i}{R}\right] \qquad 3.2\text{-}6$$

where R was measured by the longitudinal strain gauges.

The results of these "stress checks" showed that the experiments and theory still deviated considerably and that the numerical integration was not the entire reason for the discrepancies in the deflection curves.

Examination of equation 3.2-5 showed the only variable for a specific plate was k, a measure of the amount of warping of the section. Using values of k in the range $0 \leq k \leq 1.0$ agreement between theory and experiment for the bending stresses was obtained. The transverse cross section of Plate I being tested was measured and it was found that the warping at the center line corresponded to a value of k = 0.909. The bending stresses obtained from the experiments were compared to theoretical stresses calculated for k = 0.0 and k = 0.909. The two results gave closer agreement assuming k = 0.909. In a similar manner Plate II was measured and the warping found to correspond to a k = 0.727. A check of the bending stresses showed that the theoretical result for k = 0.727 gave closer agreement to the experiments than k = 0.0. Figure 3.2 and 3.3. show typical comparisons between the theoretical and experimental bending stresses.

[illegible]

[illegible]

[illegible]

[illegible]

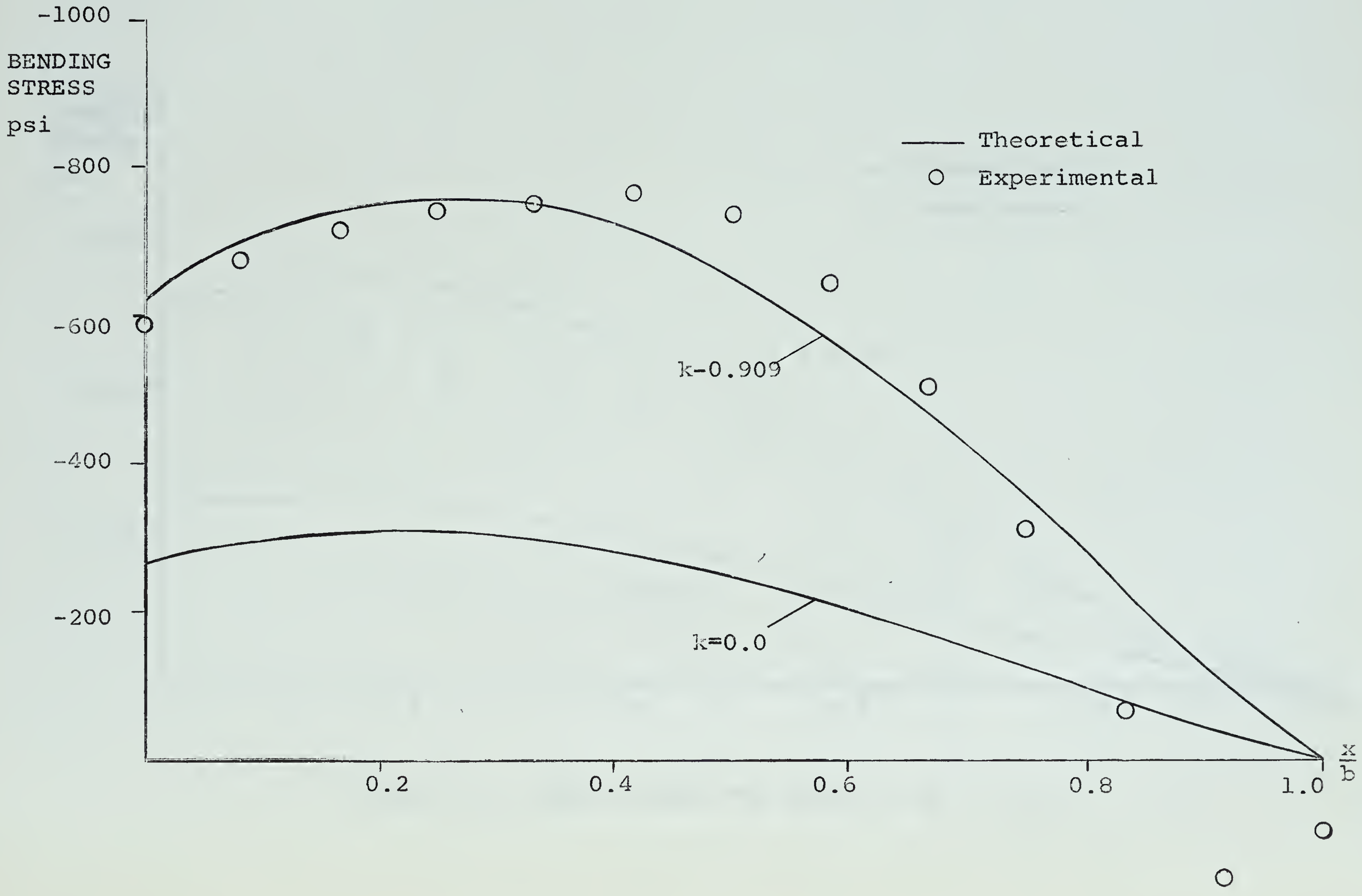

FIGURE 3.2 STRESS CHECK FOR PLATE I AT λ = 2.0

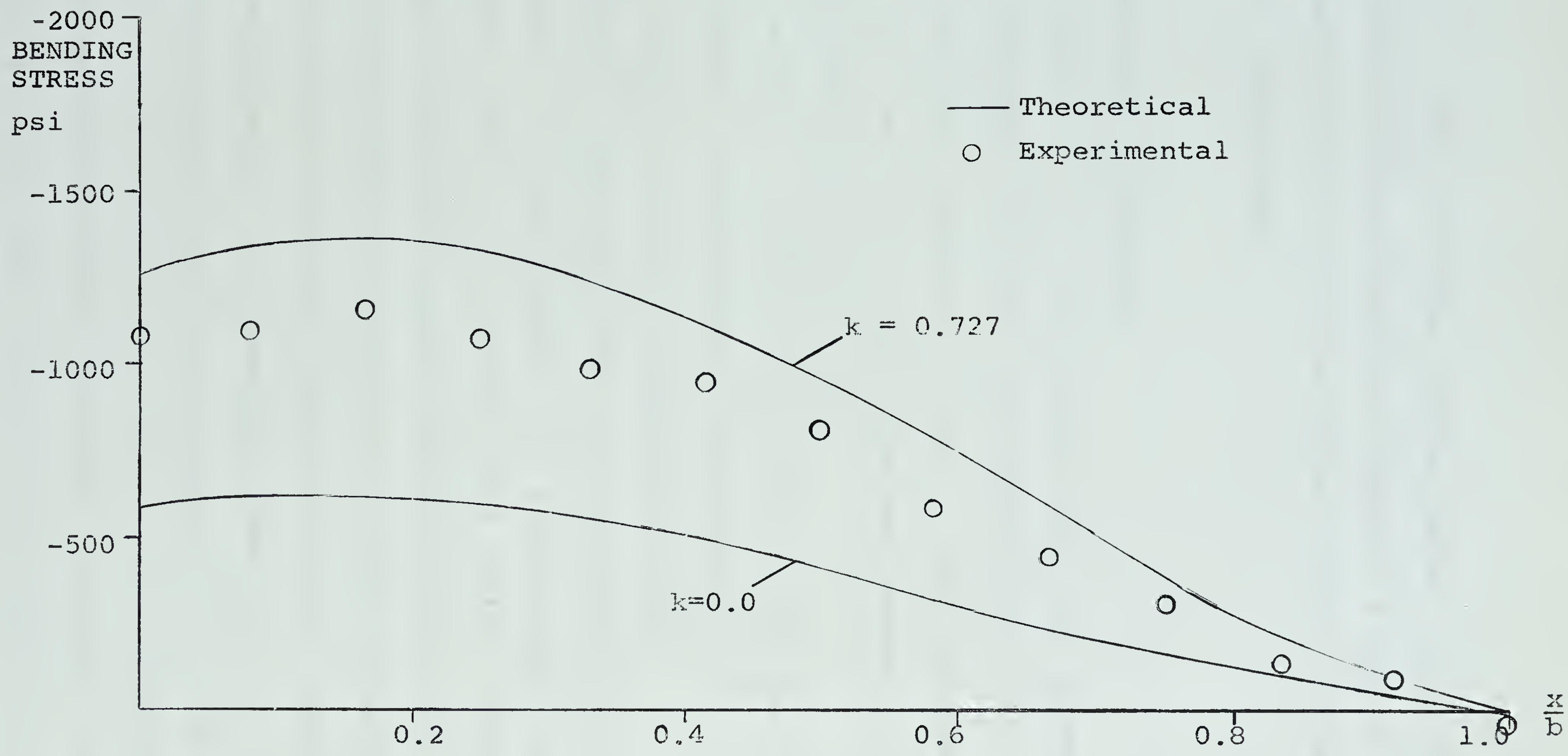

FIGURE 3.3 STRESS CHECK FOR PLATE II AT λ = 2.0

As a result of these "stress checks", the transverse deflection curves shown in figures 3.4 to 3.11 for Plate I and in 3.12 to 3.15 for Plate II use $k = 0.909$ and $k = 0.727$, respectively.

3.3 Discussion of Results

Figures 3.4 to 3.15 indicate that good agreement between experiment and theory was obtained for Plate II and for the lower λ values of Plate I. The disagreement seen at $\lambda > 3.0$ for Plate I could have been caused by some of the following sources of error:

(1) error in calibrating the digital data processor

(2) error in measurement of the strains

(3) error in using the trapezoidal rule.

Bellow[12] has shown that the calibration error for the processor was approximately ± 0.8 percent, and the measurement error was ± 0.6 percent full scale. Since at the higher λ values the strains recorded were in the order of one-quarter to one-half full scale, the measurement error was not more than approximately ± 2.5 percent. The truncation error, which resulted from using the trapezoidal rule, has been shown by Bellow[12] to be in the order of ± 0.25 percent when using a one-eighth inch plate with measuring stations one-half inch apart. The total error from the above causes was less than 4.0 per-

cent and applying this error to the values obtained made little change in the experimental results. The discrepancies in the curves for Plate I for $\lambda > 3.0$ were due to much larger errors than those discussed in this paragraph.

It was believed that the reason the deflections of Plate I obtained experimentally differed from the theoretical result was the non-uniform warping which occurred during machining. Examination of figure 2.1 shows that the assumed and actual cross sections of Plate I deviated considerably, while figure 2.2 shows that the assumed cross sectional shape of Plate II closely approximated the actual case. Since good agreement was obtained from tests on Plate II it was concluded that the discrepancies found in Plate I were due to non-uniform warping of the transverse cross section.

3.4 Conclusions

1. The theory presented in Chapter I predicted with reasonable accuracy, the experimental results of the two plates tested in the range $0 < \lambda < 4$. The discrepancies seen at the higher λ values for Plate I were probably due to the initial imperfections of this plate.

2. The earlier theoretical results of Lamb[1] for a rectangular transverse cross section, and Fung and Wittrick[7] for a double-wedge cross section were shown to be limiting cases of the theory of Chapter I.

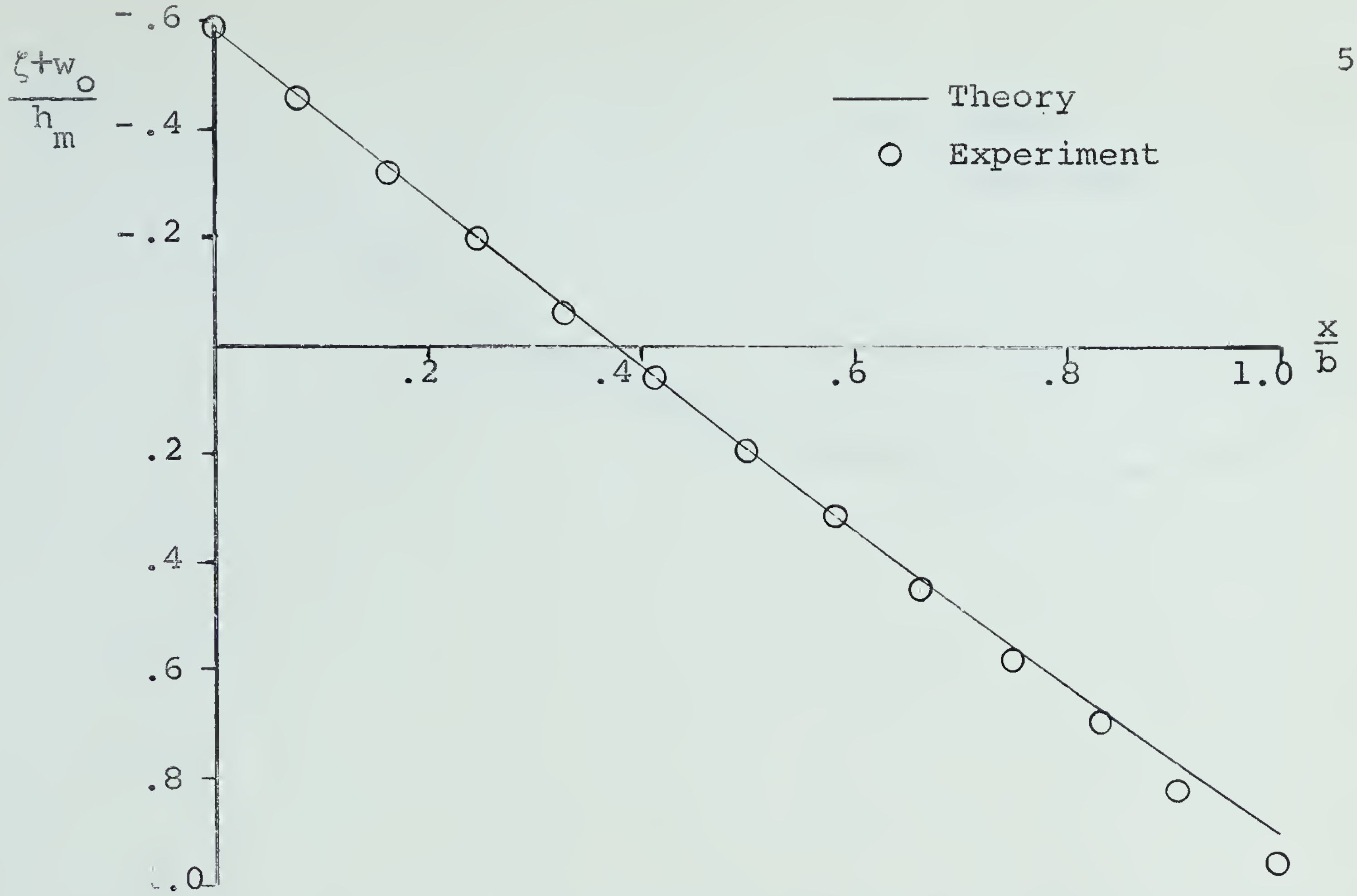

FIGURE 3.4 TRANSVERSE DEFLECTIONS FOR PLATE I AT λ = 1.0

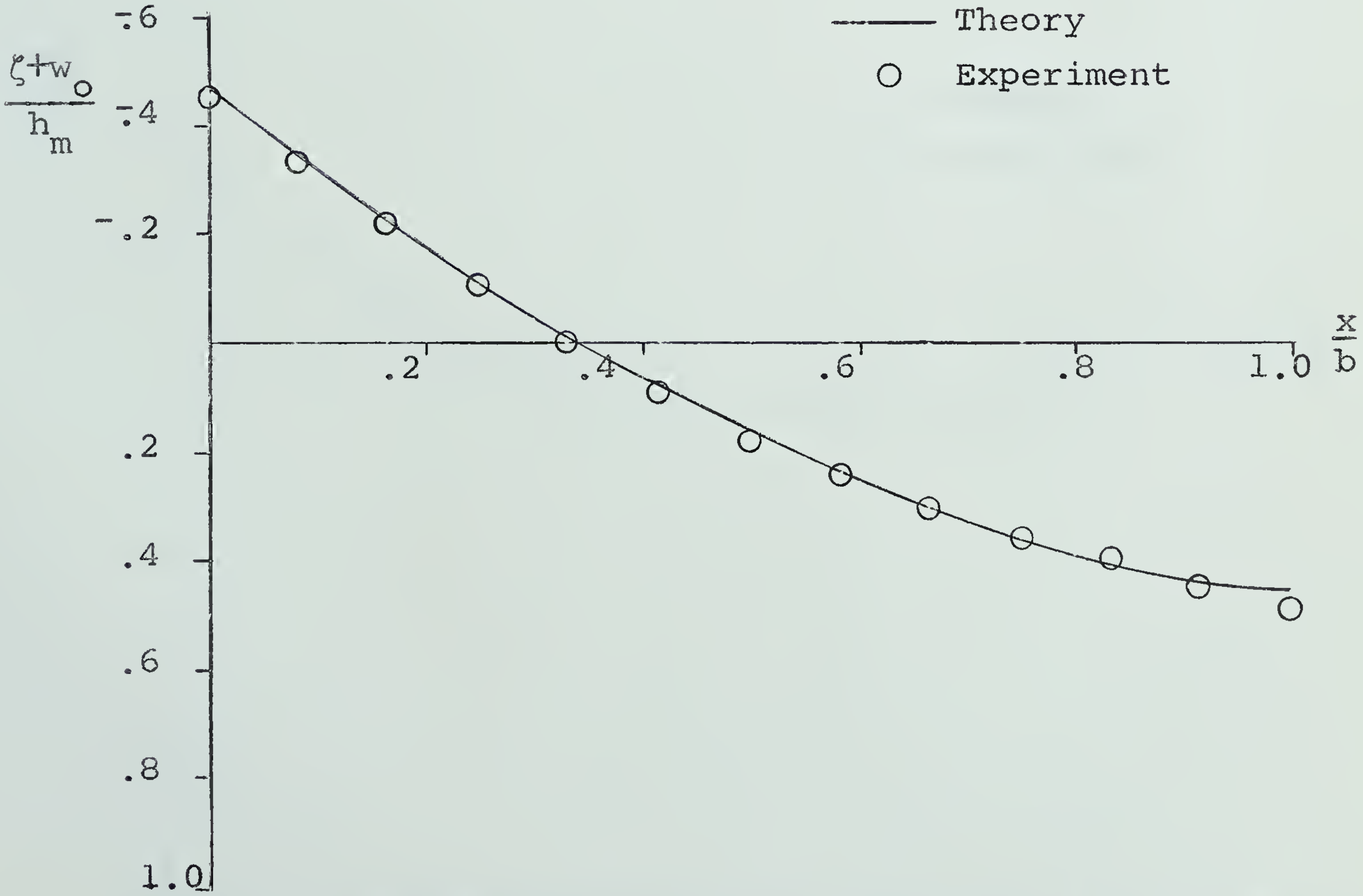

FIGURE 3.5 TRANSVERSE DEFLECTIONS FOR PLATE I AT λ = 2.0

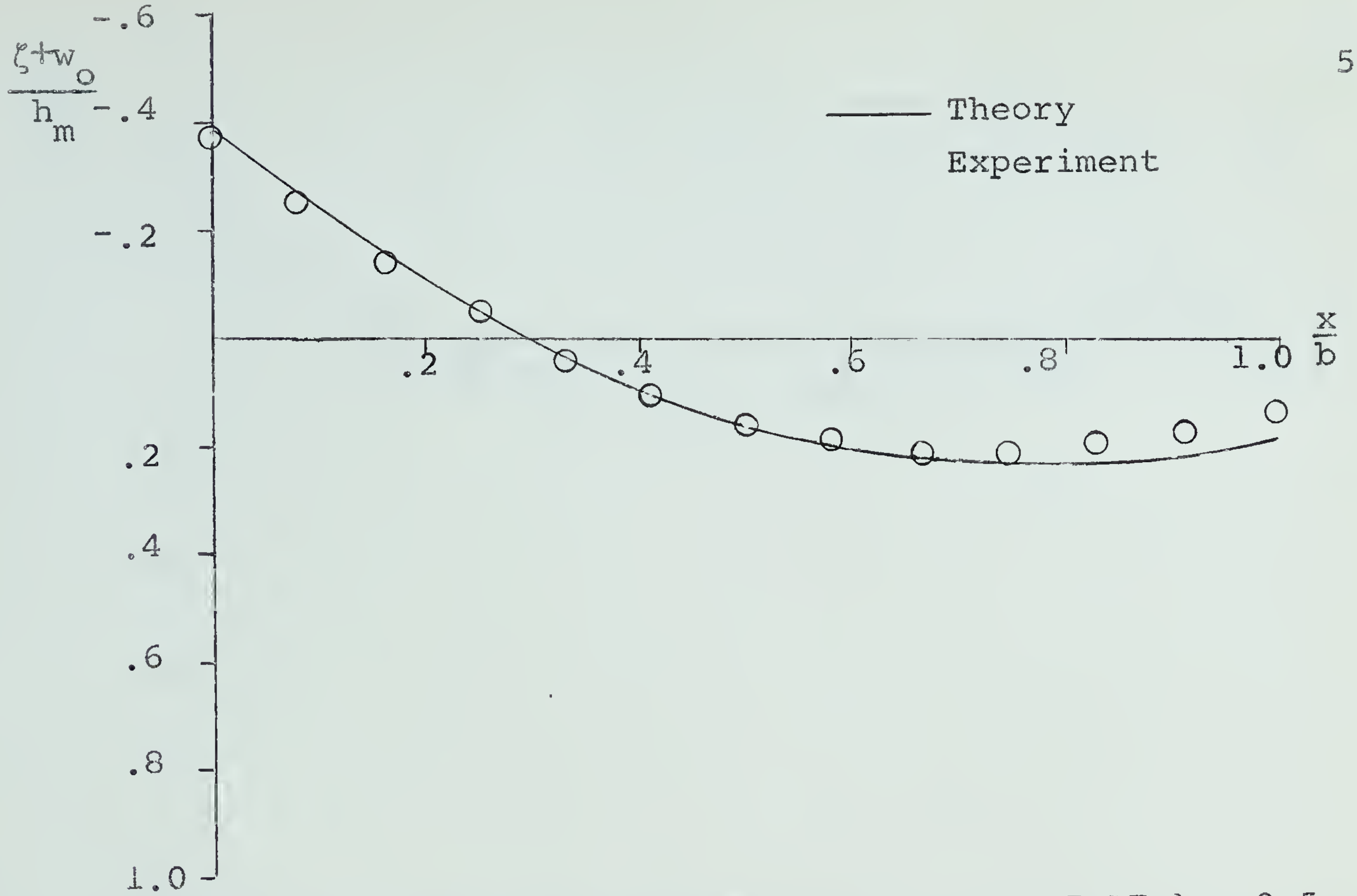

FIGURE 3.6 TRANSVERSE DEFLECTIONS FOR PLATE I AT λ = 2.5

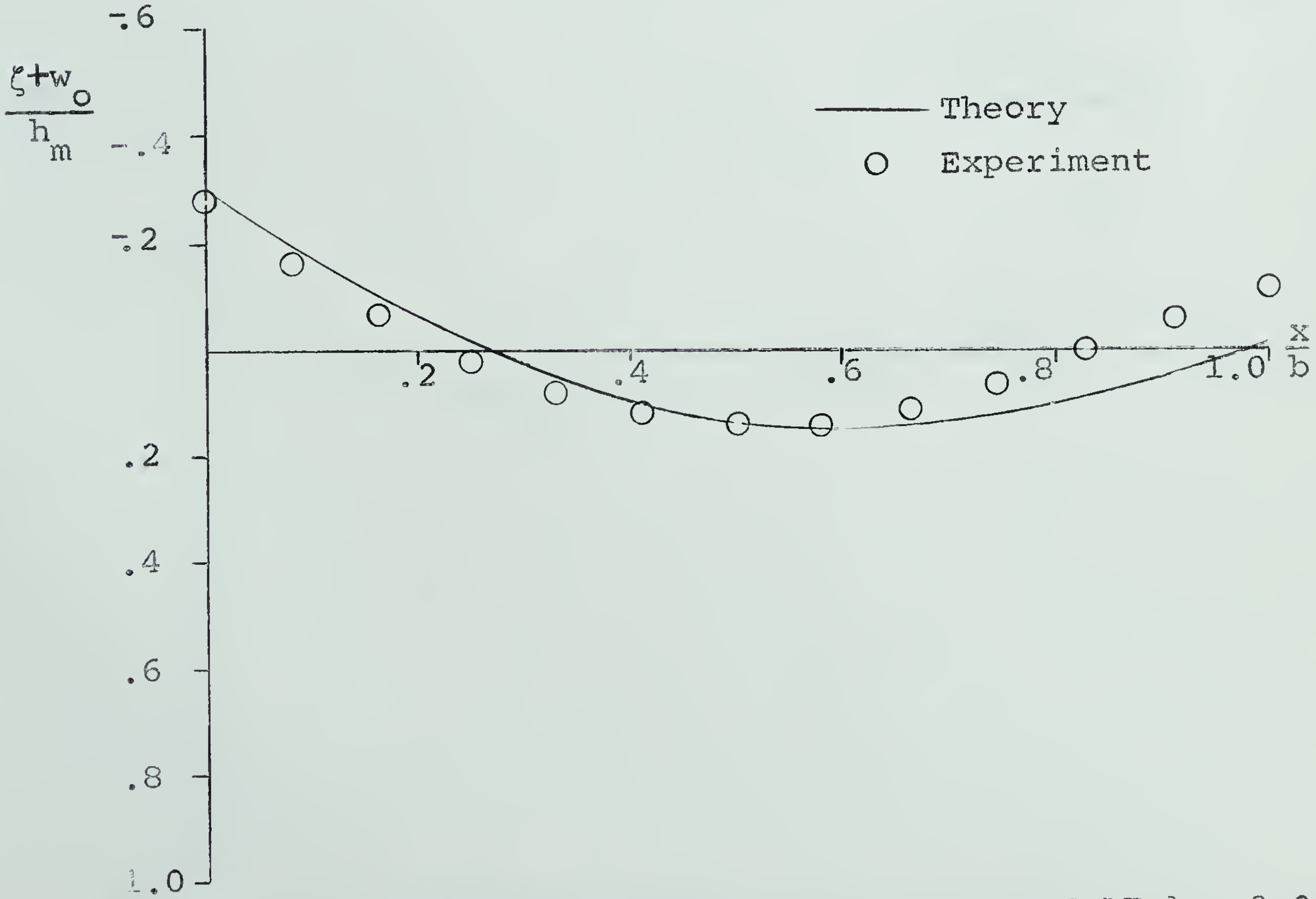

FIGURE 3.7 TRANSVERSE DEFLECTIONS FOR PLATE I AT λ = 3.0

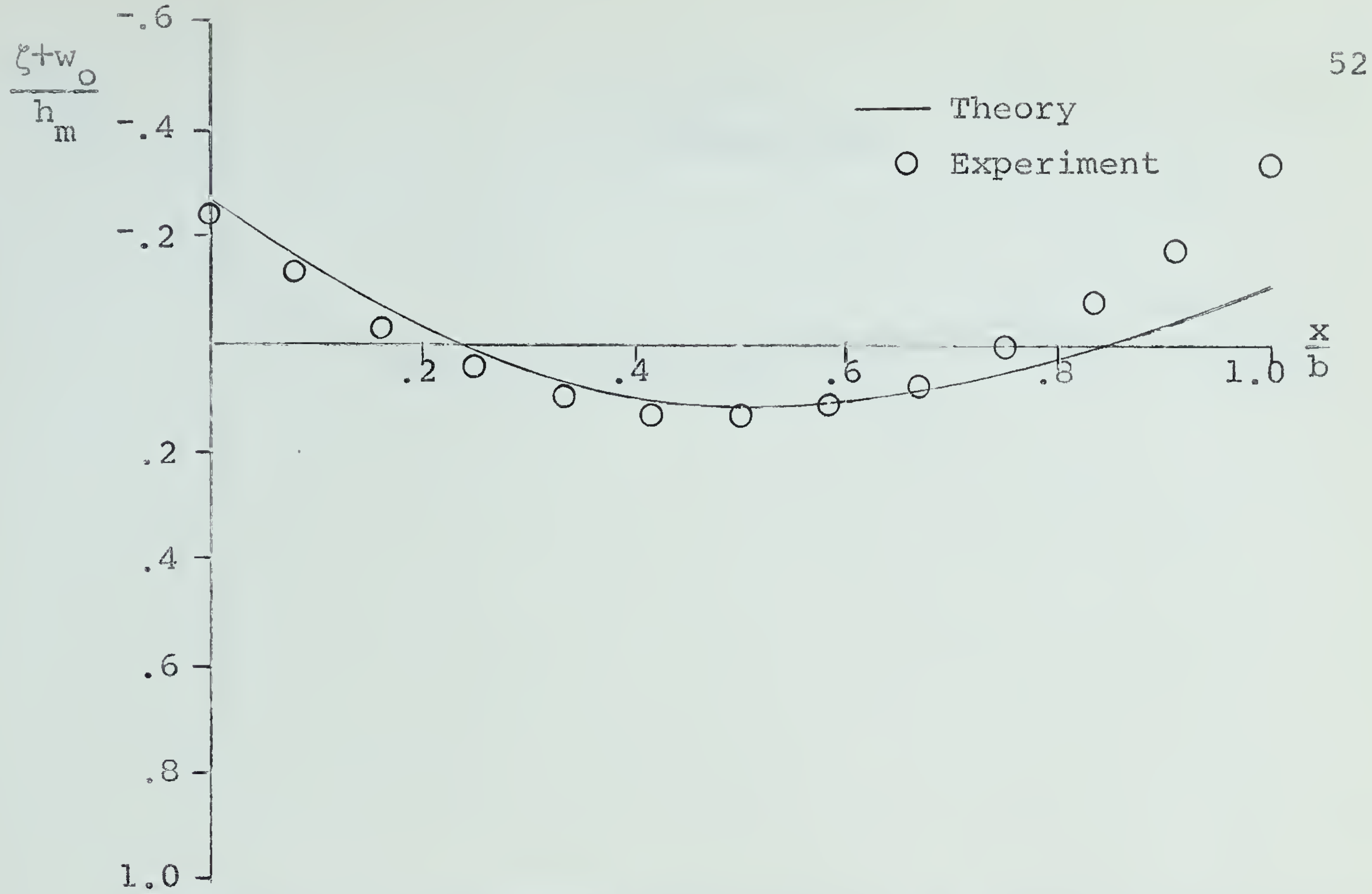

FIGURE 3.8 TRANSVERSE DEFLECTIONS FOR PLATE I AT λ = 3.5

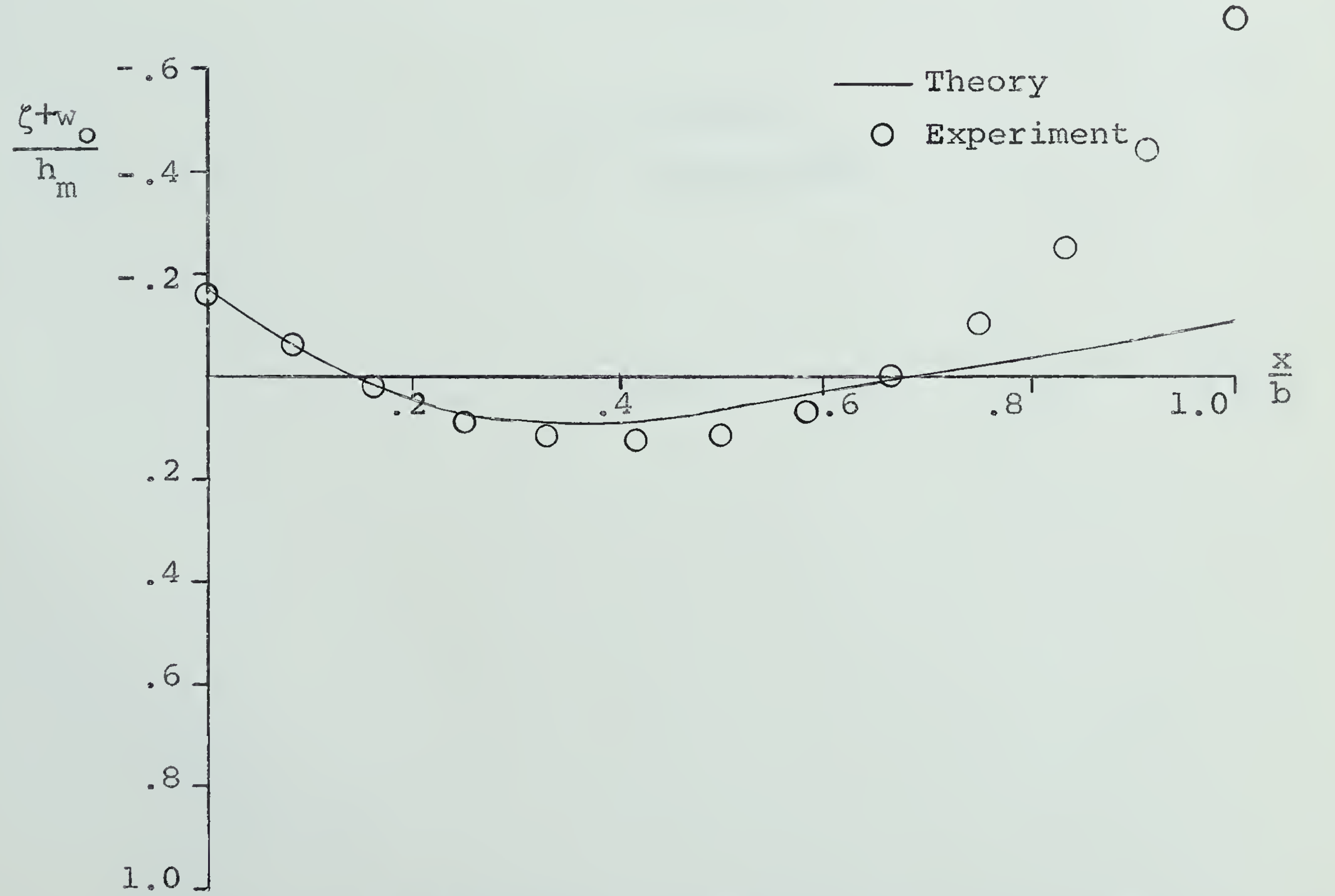

FIGURE 3.9 TRANSVERSE DEFLECTIONS FOR PLATE I AT λ = 5.0

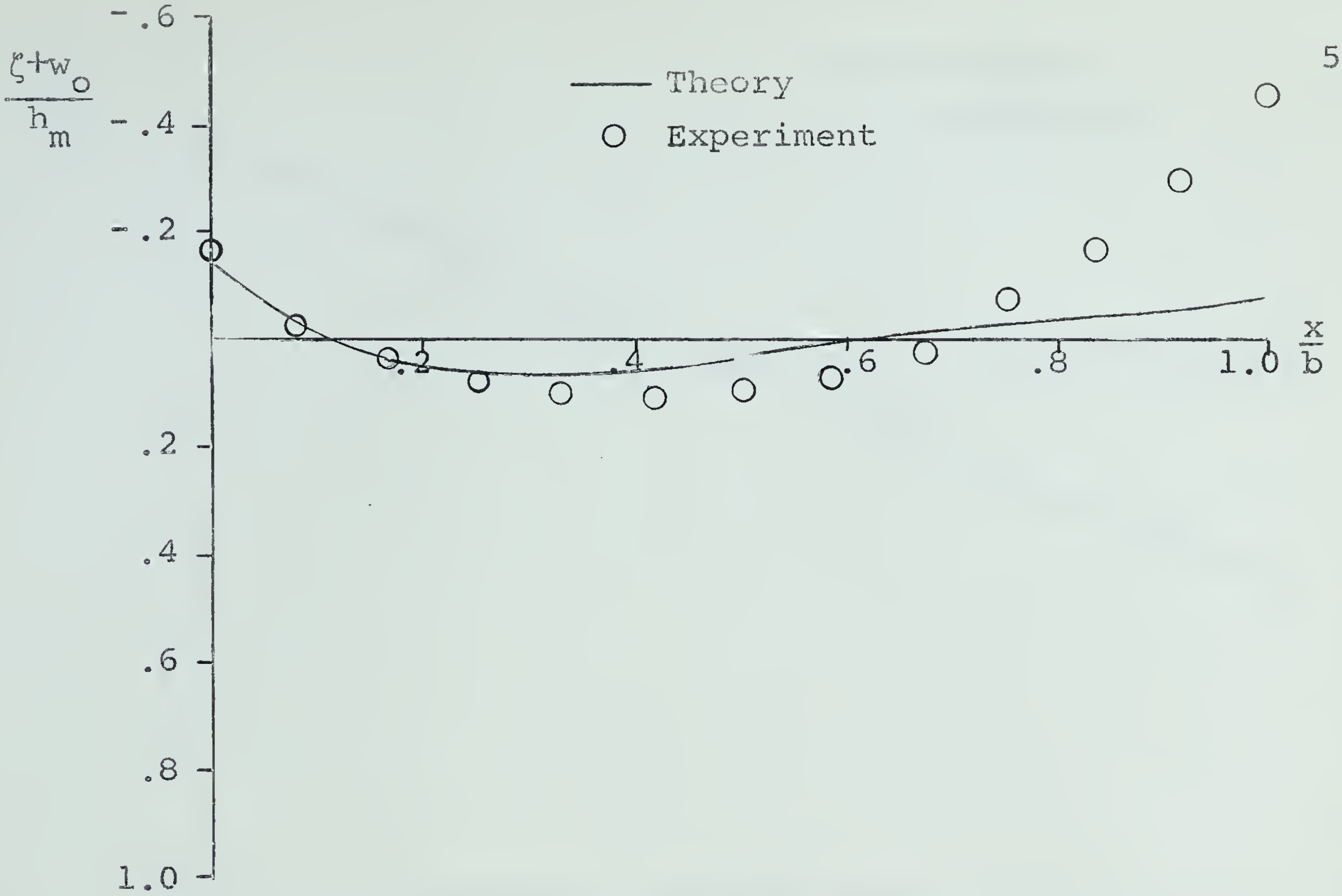

FIGURE 3-10 TRANSVERSE DEFLECTIONS FOR PLATE I AT $\lambda = 6.0$

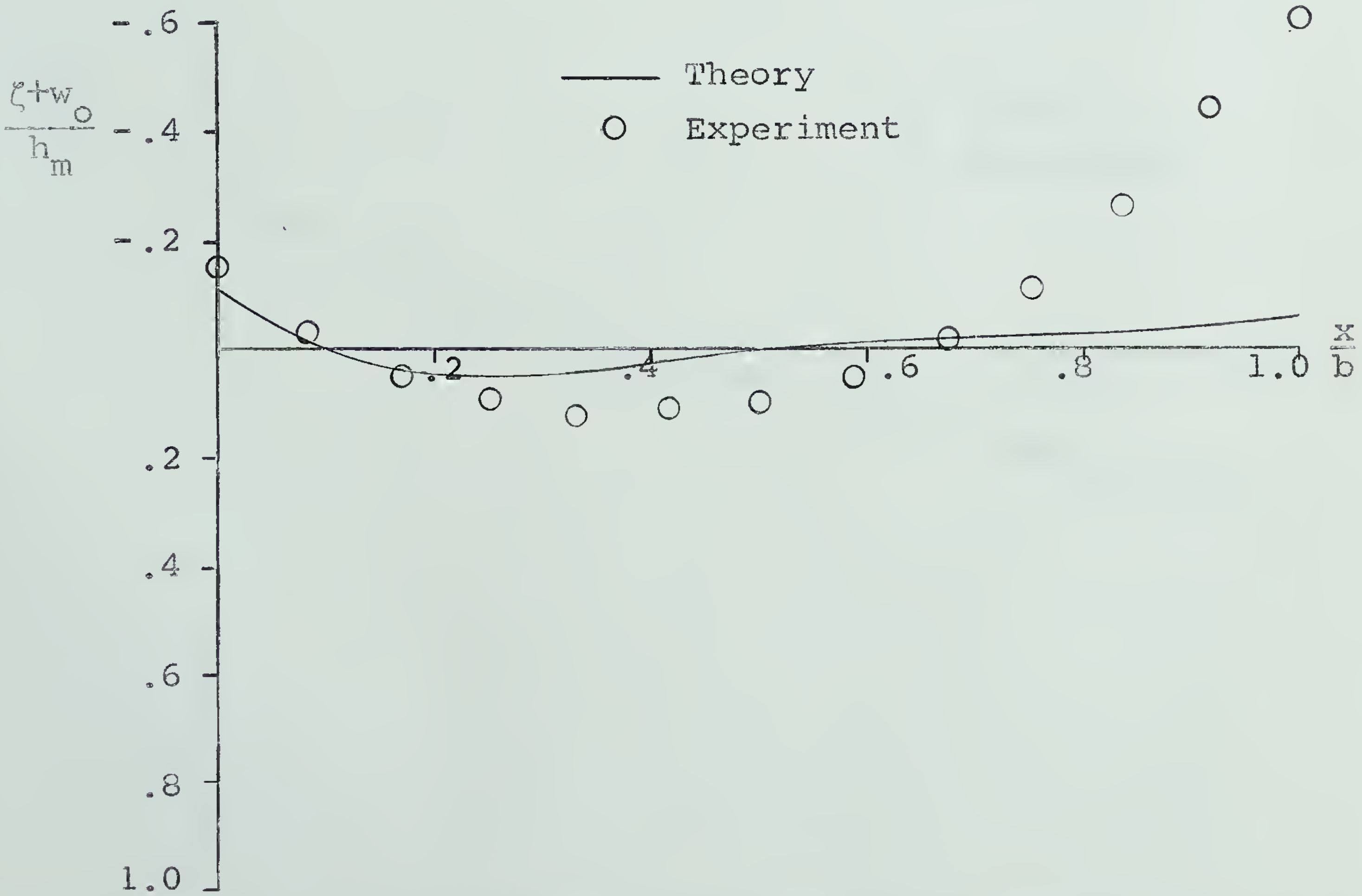

FIGURE 3-11 TRANSVERSE DEFLECTIONS FOR PLATE I AT $\lambda = 7.5$

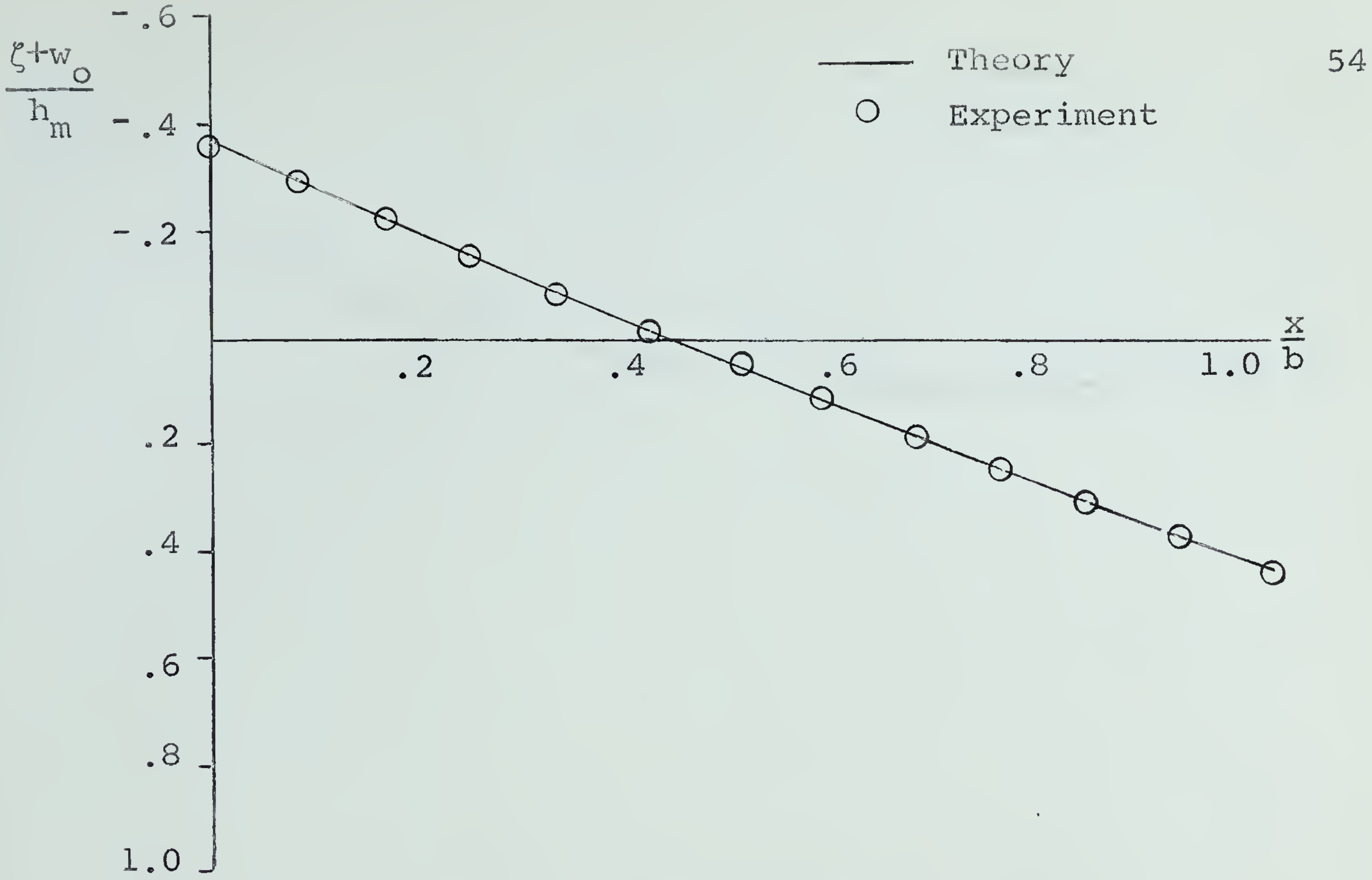

FIGURE 3-12 TRANSVERSE DEFLECTIONS FOR PLATE II AT $\lambda = 1.0$

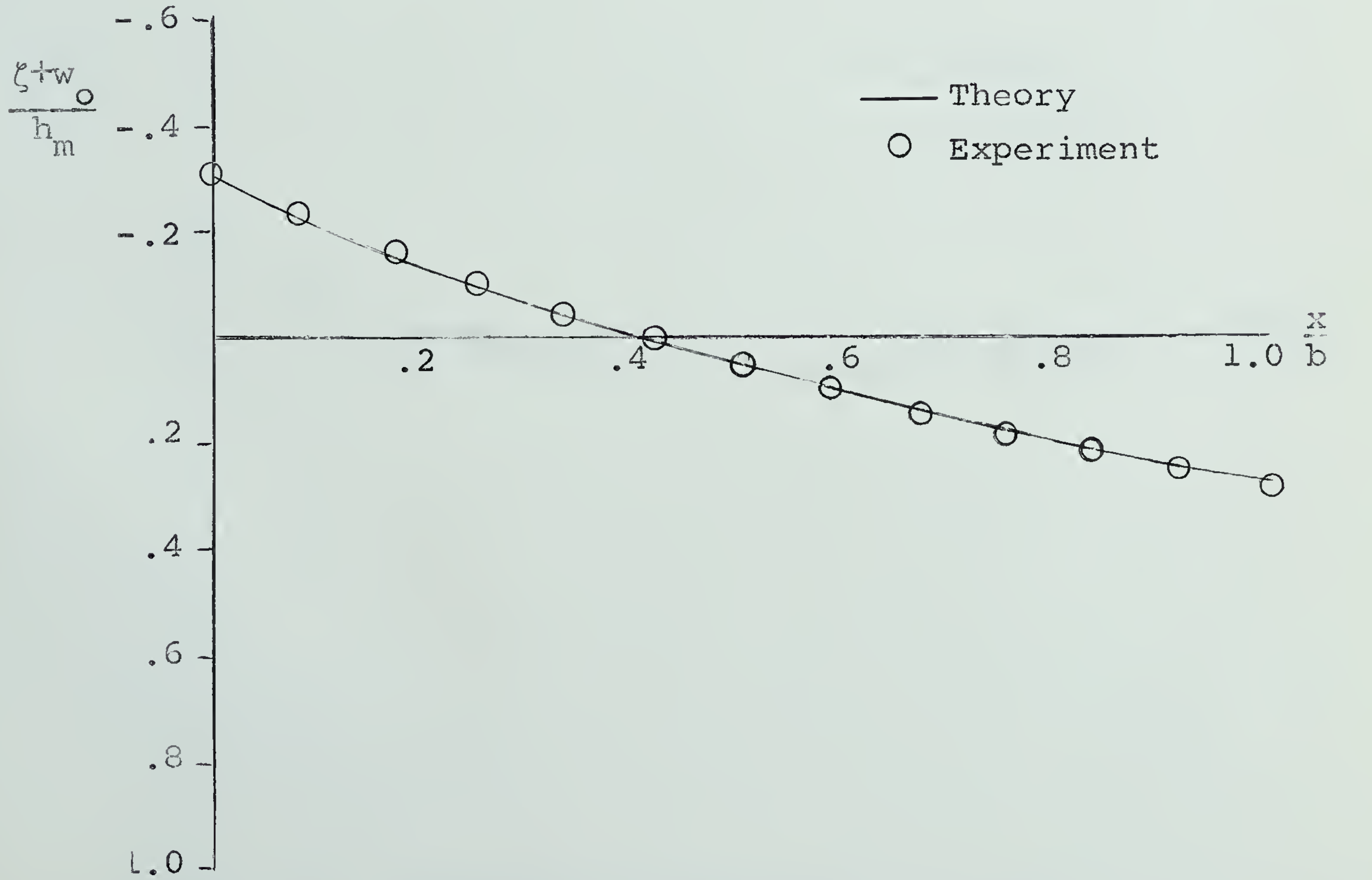

FIGURE 3-13 TRANSVERSE DEFLECTIONS FOR PLATE II AT $\lambda = 2.0$

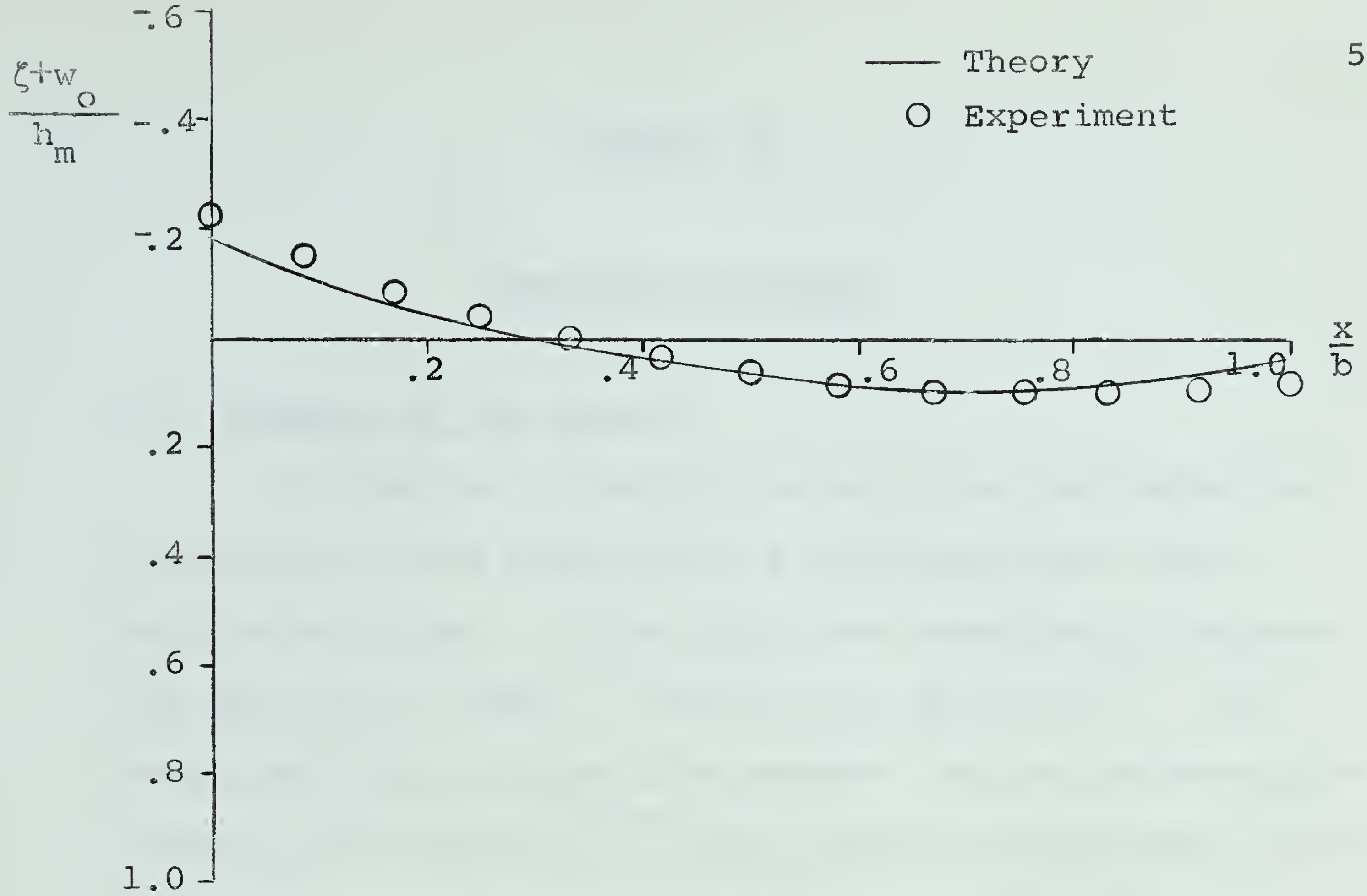

FIGURE 3-14 TRANSVERSE DEFLECTIONS FOR PLATE II AT $\lambda = 3.0$

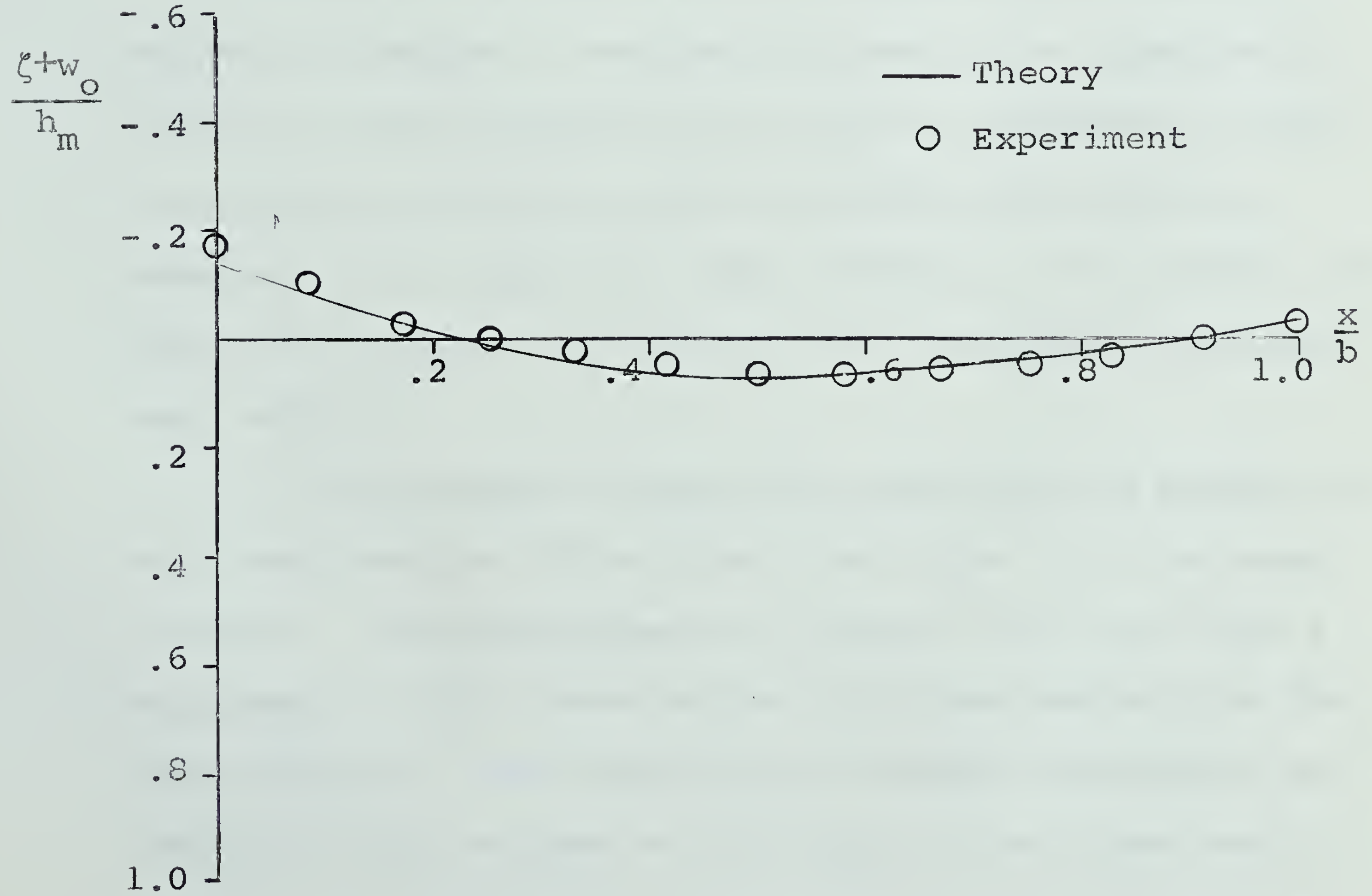

FIGURE 3-15 TRANSVERSE DEFLECTIONS FOR PLATE II AT $\lambda = 3.8$

CHAPTER IV

CONCLUDING REMARKS

4.1 Summary of the Thesis

In Chapter I theory governing the transverse deflections of thin plates with a bi-trapezoidal cross section was given. This theory was developed by extending the work of Lamb[1] and Fung and Wittrick[7]. The developed theory, which lies between the two extremes discussed by the authors[1,7], was shown to approximate these earlier results by a suitable selection of the variable parameters.

With the aid of a digital computer, the theory derived in Chapter I was used to predict the experimental results of tests carried out on two bi-trapezoidal plates. The computer was again used to integrate the strains, measured on the upper and lower surfaces of the plates, to obtain the deflection curves of the transverse cross sectional midline.

The agreement between the predicted and actual results was good for Plate II and for Plate I at the lower λ values. The disagreement at values $\lambda > 3.0$ for Plate I was thought to be caused by the non-linear warping of the cross section. The discrepancies between experiment and theory are most evident at the edges of the cross section

where pronounced distortion occurred during machining.

4.2 Practical Applications and Problems for Further Study

The theory developed above is, of course, directly applicable to other bi-trapezoidal plates with similar boundary conditions. This type of problem occurs in thin wing design as pointed out by Flugge[5]. In this case the transverse deflections can influence the bending stiffness as well as the aerodynamic qualities of the wing. Conway and Farnham[8] have discussed the transverse distortion problem in connection with magnetic tapes used in computer applications. The tapes when bent over a reading head distort causing uneven wear. Using a tape cross section other than rectangular could reduce this distortion.

The theoretical moment-curvature relationship for certain bi-trapezoidal plates has been shown by Flugge[5]. This could be extended to all bi-trapezoidal plates and the instability in the applied moment similar to that shown theoretically by Ashwell[14] for uniform thickness plates, could be investigated theoretically and experimentally.

BIBLIOGRAPHY

1. LAMB, H., "On the Flexure of a Flat Elastic Spring", Philosophical Magazine, Series 5, Vol. 31, 1891. pp182-188.

2. ASHWELL, D.G. "The Anticlastic Curvature of Rectangular Beans and Plates", Journal of the Royal Aeronautical Society, 1950, pp 782-788.

3. BELLOW, D.G., FORD, G. and KENNEDY, J.S., "Anticlastic Behaviour of Flat Plates", Experimental Mechanics, Vol. 5, 1965, pp 227-232.

4. CONWAY, H.D. and NICKOLA, W.E., "Anticlastic Action of Flat Sheets in Bending", Experimental Mechanics, Vol. 5, 1965, pp 115-119

5. FLUGGE, W., "Large Deflections of Thin Wings", Technical Report No. 3, Air Forces Contract W33-038, AC-16667, Stanford University, Stanford, California, 1949.

6. MURRAY, T.R. and NILES, A.S., "Bending of Wide Beams of Doubly Symmetric Section", Technical Report No. 4, Air Forces Contract W33-038, AC-16667, Stanford University, Stanford, California, 1949.

7. FUNG, Y.C. and WITTRICK, W.H., "The Anticlastic Curvature of a Strip with Lateral Thickness Variation", Journal of Applied Mechanics, Vol. 21, 1954.

8. CONWAY, H.D. and FARNHAM, K.A., "Anticlastic Curvature of Strips of Variable Thickness", International Journal of Mechanical Sciences, Vol. 7, 1965, pp 451-458.

9. TIMOSHENKO, S.P. and WOINOWSKY-KRIEGER, S., Theory of Plates and Shells, McGraw-Hill, 1959, pp488-497.

10. FLUGGE, W., Stresses in Shells, Springer-Verlag, 1962, pp 287-293.

11. McLACHLAN, N.W., Bessel Functions for Engineers, Oxford University Press, 1955, pp 137-152.

[illegible]

[illegible]

[illegible]

[illegible]

[illegible]

[illegible]

[illegible]

[illegible]

[illegible]

[illegible]

[illegible]

[illegible]

[illegible]

12. BELLOW, D.G., Anticlastic Behaviour of Flat Plates, Unpublished Ph.D. Thesis, University of Alberta, 1963.

13. CRANDALL, S.H., Engineering Analysis, McGraw-Hill, 1956, p 160

14. ASHWELL, D.G., "A Characteristic Type of Instability in the Large Deflections of Elastic Plates, I. Curved Rectangular Plates Bent About One Axis", Proceedings of the Royal Society, A, Vol. 214, pp 98-109.

APPENDIX I

FORTRAN IV PROGRAM FOR EVALUATION OF DEFLECTIONS AND BENDING STRESSES.

In Chapter I the solution of the differential equation for the transverse distortion of a bi-trapezoidal plate was shown to be

$$\zeta = \frac{1}{\eta}\left[S\ \mathrm{ber}'\eta + T\ \mathrm{bei}'\eta + U\ \mathrm{ker}'\eta + V\ \mathrm{kei}'\eta \right]$$

$$- w_o - \frac{6\mu b^2}{\lambda^4 R}$$

The program shown below solves equations 1.2-20a to 1.2-23a for the constants S,T,U and V. This is accomplished through the use of a subroutine called SUBROUTINE SOLVE (shown below). These values of S, T, U and V, called X(1) to X(4) in the program are used in calculating the distortion ζ. The deflection of the midline of the cross section, $w = \zeta + w_o$, is calculated and made non-dimensional by dividing by h_m half the total maximum thickness of the plate. Finally the bending stresses, called SX(J) are computed using equation 3.1-5.

The values of the Thomson functions, and their first derivatives were calculated by using a series or an asymptotic expansion depending on the value of the argument.

If the value of the argument was in the range $0 < \eta \leq 8$ power series* were used and if $\eta > 8$ the asymptotic expansions* were used. The asymptotic expansions were needed since the series used diverge rapidly for arguments above 8. The values of the Thomson functions given by the expansions in the range $8 < \eta < 10$ are not precise and vary up to approximately 10 per cent from those found in published tables**. However, this error was not noticeable in the portion of the deflection curves calculated using these expansions.

The program, which was run on the University of Alberta's IBM 7040/1401 system could be improved. The series and asymptotic expansions used were computed three different times in the program. These series and expansions should have been in a subroutine and called for when values were desired. A recursion formula could have been used in place of actually including the series terms in the program. This would save computer time as well as increasing the accuracy of the results.

---

* Obtained from Handbook of Mathematical Functions, U.S. Department of Commerce, National Bureau of Standards, Applied Mathematics Series 55, pp 384-385.

** Dwight, H.B., Mathematical Tables, Dover, 1961, pp 193-204.

An explanation of the symbols used for the input data appear below:

BB - the square of half the plate width

YM - Young's Modulus x 10^{-6}

NN - number of measuring points on half the cross section for which values are desired

SMU - Poisson's ratio

TO - t_o

C - edge thickness

FLA - lambda value

OK - k

The results appear in two columns; the first is the non-dimensional deflections and the second the bending stresses in psi.

```
      DIMENSION Z(20),V(30),B(30),E(30),D(20)
      COMMON A(6,6),N,X(6)
      READ (5,63) BB,YM
   63 FORMAT(2F7.2)
   91 READ(5,92) NN,SMU,TO,C,FLA,OK
   92 FORMAT (I4,3F9.4,2F7.3)
      WRITE(6,93) FLA,OK
   93 FORMAT (8H LAMBDA=,F7.3,3H K=,F7.3)
    3 EP=2.*FLA*(C/(2.*TO))**0.5
      ALP=2.*FLA*(1.+C/(2.*TO))**0.5
      RAD=SQRT(3.*(1.-SMU*SMU))*BB/(FLA*FLA*TO)
      BET=C/(2.*TO)
      PI=3.14159
      R=1.41421
      P=PI/8.
      EZ=EP/8.
      AZ=ALP/8.
      IF(EP.GE.8.)GO TO 6
      DO 76 KK=2,28,2
   76 E(KK)=EZ**KK
      ELOG=-ALOG(EP/2.)
      ABE=1.-64.*E(4)+113.77778*E(8)-32.36346*E(12)+2.64191*E(16)
      BERE=-.08350*E(20)+.00123*E(24)-.00001*E(28)+ABE
      ABI=16.*E(2)-113.77778*E(6)+72.81778*E(10)-10.56766*E(14)
      BEIE=.52186*E(18)-.01104*E(22)+.00011*E(26)+ABI
      ASK=ELOG*BERE+PI/4.*BEIE-.57722-59.0582*E(4)+171.36272*E(8)
      BSK=-60.60977*E(12)+5.65539*E(16)-.19637*E(20)+.0031*E(24)
      SKEE=-.00002*E(28)+ASK+BSK
      DSK=ELOG*BEIE-PI/4.*BERE+6.76455*E(2)-142.91828*E(6)
      ESK=124.23570*E(10)-21.3006*E(14)+1.17509*E(18)-.02696*E(22)
      SKIE=.00030*E(26)+DSK+ESK
      BER1=EP*(-4.*E(2)+14.22222*E(6)-6.06815*E(10)+.66048*E(14))
      BRPE=EP*(-.02609*E(18)+.00046*E(22))+BER1
      BEI1=EP*(0.5-10.66667*E(4)+11.37778*E(8)-2.31168*E(12))
      BIPE=EP*(.14677*E(16)-.00379*E(20)+.00004*E(24))+BEI1
      SKRP1=ELOG*BRPE-BERE/EP+PI/4.*BIPE+EP*(-3.69114*E(2))
      SKRP2=EP*(21.42034*E(6)-11.36433*E(10)+1.41385*E(14)-.06163*E(18))
      SKRPE=EP*(.00116*E(22)-.00001*E(26))+SKRP1+SKRP2
      SKI2=ELOG*BIPE-BEIE/EP-PI/4.*BRPE+.21139*EP
      SKI3=EP*(-13.39859*E(4)+19.41183*E(8)-4.65951*E(12)+.33049*E(16))
      SKIPE=EP*(-.00927*E(20)+.00011*E(24))+SKI2+SKI3
      GO TO 5
```

```
 6 TPE=(2.*PI*EP)**(-0.5)
   PSE=SQRT(PI/(2.*EP))
   EXO=EXP(EP/R)
   EXM=EXP(-EP/R)
   BERE=TPE*EXO*COS(EP/R-P)
   BEIE=TPE*EXO*SIN(EP/R-P)
   SKEE=PSE*EXM*COS(EP/R+P)
   SKIE=-PSE*EXM*SIN(EP/R+P)
   BRPE=TPE*EXO*COS(EP/R+P)
   BIPE=TPE*EXO*SIN(EP/R+P)
   SKRPE=-PSE*EXM*COS(EP/R-P)
   SKIPE=PSE*EXM*SIN(EP/R-P)
 5 IF(ALP.GE.8.)GO TO 8
   DO 74 JJ=2,28,2
74 B(JJ)=AZ**JJ
   PLOG=-ALOG(ALP/2.)
   ABA=1.-64.*B(4)+113.77778*B(8)-32.36346*B(12)+2.64191*B(16)
   BERA=-.08350*B(20)+.00123*B(24)-.00001*B(28)+ABA
   ACI=16.*B(2)-113.77778*B(6)+72.81778*B(10)-10.56766*B(14)
   BEIA=.52186*B(18)-.01104*B(22)+.00011*B(26)+ACI
   XSK=PLOG*BERA+PI/4.*BEIA-.57722-59.05820*B(4)
   YSK=171.36272*B(8)-60.60977*B(12)+5.65539*B(16)-.19637*B(20)
   SKEA=.0031*B(24)-.00002*B(28)+XSK+YSK
   ZSK=PLOG*BEIA-PI/4.*BERA+6.76455*B(2)-142.91828*B(6)
   ETK=124.2357*B(10)-21.3006*B(14)+1.17509*B(18)-.02696*B(22)
   SKIA=.00030*B(26)+ZSK+ETK
   BEP1=ALP*(-4.*B(2)+14.22222*B(6)-6.06815*B(10)+.66048*B(14))
   BRPA=ALP*(-.02609*B(18)+.00046*B(22))+BEP1
   BIP1=ALP*(0.5-10.66667*B(4)+11.37778*B(8)-2.31168*B(12))
   BIPA=ALP*(.14677*B(16)-.00379*B(20)+.00004*B(24))+BIP1
   SPA=PLOG*BRPA-BERA/ALP+PI/4.*BIPA+ALP*(-3.69114*B(2))
   TP=ALP*(21.42034*B(6)-11.36343*B(10)+1.41385*B(14)-.06163*B(18))
   SKRPA=ALP*(.00116*B(22)-.00001*B(26))+SPA+TP
   EPA=PLOG*BIPA-BEIA/ALP-PI/4.*BRPA+.21139*ALP
   FP=ALP*(-13.39859*B(4)+19.41183*B(8)-4.65951*B(12)+.33049*B(16))
   SKIPA=ALP*(-.00927*B(20)+.00011*B(24))+EPA+FP
   GO TO 9
 8 TPA=(2.*PI*ALP)**(-0.5)
   PSA=SQRT(PI/(2.*ALP))
   EXA=EXP(ALP/R)
   EXB=EXP(-ALP/R)
   BERA=TPA*EXA*COS(ALP/R-P)
   BEIA=TPA*EXA*SIN(ALP/R-P)
   SKEA=PSA*EXB*COS(ALP/R+P)
   SKIA=-PSA*EXB*SIN(ALP/R+P)
   BRPA=TPA*EXA*COS(ALP/R+P)
   BIPA=TPA*EXA*SIN(ALP/R+P)
   SKRPA=-PSA*EXB*COS(ALP/R-P)
   SKIPA=PSA*EXB*SIN(ALP/R-P)
```

```
 9 A(1,1)=-ALP*BEIA-2.*BRPA
   A(1,2)=ALP*BERA-2.*BIPA
   A(1,3)=-ALP*SKIA-2.*SKRPA
   A(1,4)=ALP*SKEA-2.*SKIPA
   A(1,5)=+2.*TO*ALP**3/(4.*FLA*FLA)*(1.+OK)
   EP2=EP*EP
   EP3=EP**3
   ALP2=ALP*ALP
   ALP3=ALP**3
   A(2,1)=4.*EP*BEIE-EP2*BIPE+8.*BRPE
    A(2,2)=-4.*EP*BERE+EP2*BRPE+8.*BIPE
    A(2,3)=4.*EP*SKIE-EP2*SKIPE+8.*SKRPE
    A(2,4)=-4.*EP*SKEE+EP2*SKRPE+8.*SKIPE
    A(2,5)=+SMU*BB*BET/(RAD*FLA*FLA)*EP3
    A(3,1)=-EP3*BERE-24.*EP*BEIE-48.*BRPE+8.*EP2*BIPE
    A(3,2)=-EP3*BEIE+24.*EP*BERE-48.*BIPE-8.*EP2*BRPE
    A(3,3)=-EP3*SKEE-24.*EP*SKIE-48.*SKRPE+8.*EP2*SKIPE
    A(3,4)=-EP3*SKIE+24.*EP*SKEE-48.*SKIPE-8.*EP2*SKRPE
    A(3,5)=0.
    A(4,1)=ALP2*BERA-2.*ALP*BIPA-EP2*BERE+2.*EP*BIPE
    A(4,2)=ALP2*BEIA+2.*ALP*BRPA-EP2*BEIE-2.*EP*BRPE
    A(4,3)=ALP2*SKEA-2.*ALP*SKIPA-EP2*SKEE+2.*EP*SKIPE
    A(4,4)=ALP2*SKIA+2.*ALP*SKRPA-EP2*SKIE-2.*EP*SKRPE
    A(4,5)=(-1.5)*SMU*TO*(ALP**4-EP**4)/(FLA*FLA*SQRT(3.-3.*SMU*SMU))
   N=4
   CALL SOLVE
   NW=NN+1
   DO 99 J=1,NW
   BJ=J-1
   BN=NN
   ETA=2.*FLA*SQRT(1.-BJ/BN+C/(2.*TO))
   VA=ETA/8.
   IF(ETA.GE.8.)GO TO 12
   DO 78 K=2,28,2
78 V(K)=VA**K
   XLOG=-ALOG(ETA/2.)
   BPN1=ETA*(-4.*V(2)+14.22222*V(6)-6.06815*V(10)+.66048*V(14))
    BRPN=ETA*(-.02609*V(18)+.00046*V(22))+BPN1
   BPN2=ETA*(0.5-10.66667*V(4)+11.37778*V(8)-2.31168*V(12))
   BIPN=ETA*(.14677*V(16)-.00379*V(20)+.00004*V(24))+BPN2
   BRA=1.-64.*V(4)+113.77778*V(8)-32.36346*V(12)+2.64191*V(16)
    BERN=-.08350*V(20)+.00123*V(24)-.00001*V(28)+BRA
   BIN=16.*V(2)-113.77778*V(6)+72.81778*V(10)-10.56766*V(14)
   BEIN=.52185*V(18)-.01104*V(22)+.00011*V(26)+BIN
   SPN=XLOG*BRPN-BERN/ETA+PI/4.*BIPN+ETA*(-3.69114*V(2))
   TNT=ETA*(21.42034*V(6)-11.36343*V(10)+1.41385*V(14)-.06163*V(18))
   SKRPN=ETA*(.00116*V(22)-.00001*V(26))+SPN+TNT
   EPN=XLOG*BIPN-BEIN/ETA-PI/4.*BRPN+ETA*.21139
   FN=ETA*(-13.39859*V(4)+19.41183*V(8)-4.65951*V(12)+.33049*V(16))
```

```
      SKIPN=ETA*(-.00927*V(20)+.C0011*V(24))+EPN+FN
      XSK=XLOG*BERN+PI/4.*BEIN-.57722-59.0582*V(4)+171.36272*V(8)
      YS=-60.60977*V(12)+5.65539*V(16)-.19637*V(20)+.0031*V(24)
      SKEN=-.00002*V(28)+XSK+YS
      DEK=XLOG*BEIN-PI/4.*BERN+6.76455*V(2)-142.91828*V(6)
      EEK=124.23570*V(10)-21.3006*V(14)+1.17509*V(18)-.02696*V(22)
      SKIN=.00030*V(26)+DEK+EEK
      GO TO 13
   12 TPN=(2.*PI*ETA)**(-0.5)
      PSN=SQRT(PI/(2.*ETA))
      EXC=EXP(ETA/R)
      EXD=EXP(-ETA/R)
      BRPN=TPN*EXC*COS(ETA/R+P)
      BIPN=TPN*EXC*SIN(ETA/R+P)
      SKRPN=-PSN*EXD*COS(ETA/R-P)
      SKIPN=PSN*EXD*SIN(ETA/R-P)
      BERN=TPN*EXC*COS(ETA/R-P)
      BEIN=TPN*EXC*SIN(ETA/R-P)
      SKEN=PSN*EXD*COS(ETA/R+P)
      SKIN=-PSN*EXD*SIN(ETA/R+P)
   13 F=C/(2.*TO)
      GAMK=TO*(1.-BJ/BN+F)*(1.+OK)-OK*C/2.
      CONT=TO*(2.*(1.+OK)/3.+1.*F*(2.+OK)+2.*F*F)/(2.*F+1.)
      WO=-1.*(GAMK-CONT)
      VLT=6.*SMU*TO/(FLA*FLA*SQRT(3.-3.*SMU*SMU))
      Z(J)=1./ETA*(X(1)*BRPN+X(2)*BIPN+X(3)*SKRPN+X(4)*SKIPN)-WO-VLT
      D(J)=(Z(J)+WO)/(TO+C/2.)
      DIMENSION W(5),SX(20)
      T=2.*TO*(1.-BJ/BN)+C
      DO 67 KE=1,5
   67 W(KE)=ETA**KE
      FTD=X(1)*(4.*W(1)*BEIN-W(2)*BIPN+8.*BRPN)
      STD=X(2)*(-4.*W(1)*BERN+W(2)*BRPN+8.*BIPN)
      TTD=X(3)*(4.*W(1)*SKIN-W(2)*SKIPN+8.*SKRPN)
      ATD=X(4)*(-4.*W(1)*SKEN+W(2)*SKRPN+8.*SKIPN)
      CON=4.*FLA**4/(BB*W(5))
      SDZ=CON*(FTD+STD+TTD+ATD)
      FC=+YM*(1.E06)*T/(2.*(1.-SMU*SMU))
      SX(J)=FC*(SDZ+SMU/RAD)
      WRITE (6,45) D(J),SX(J)
   45 FORMAT(1X,F10.5,10X,F10.2)
   99 CONTINUE
      GO TO 91
      END
```

```
      SUBROUTINE SOLVE
      COMMON A(6,6),N,X(6)
      LOGICAL SING
      SING=.FALSE.
      M=N+1
      NM1=N-1
      DO 1 I=1,N
1     A(I,M)=-A(I,M)
      DO 20 I=1,NM1
      AMAX = A(I,I)
      K=I
      DO 19 J= I,N
      IF (ABS (A(J,I)).LE.ABS (AMAX )) GO TO 19
      AMAX = A(J,I)
      K=J
19    CONTINUE
      IF ( AMAX.NE.0.0) GO TO 30
      SING = .FALSE.
      RETURN
30    IF ( ABS(AMAX).GE.0.1E-20) GO TO 31
      WRITE (6,14)
14    FORMAT (1HJ,14X,45H MATRIX IS EITHER SINGULAR OR ILL CONDITIONED)
31    DO 18 J=I,M
      TS = A(I,J)
      A(I,J) = A(K,J)
18    A(K,J)=TS
      IP1 = I+1
      DO 11 J=IP1,N
      FMULTP = A(J,I)/A(I,I)
      DO 11 L=IP1,M
11    A(J,L) = A(J,L) - FMULTP * A(I,L)
20    CONTINUE
      X(N) = A(N,M)/A(N,N)
      DO 22 I=1,NM1
      K = N-I
      KP1 = K+1
      FNUM = 0.0
      DO 23 J = KP1,N
23    FNUM = FNUM + X(J)*A(K,J)
22    X(K)=(A(K,M)-FNUM)/A(K,K)
      RETURN
      END
```

APPENDIX II

FORTRAN IV PROGRAM FOR CALCULATION OF EXPERIMENTAL RESULTS

The IBM 7040/1401 was again used to numerically integrate the curvatures obtained from tests on the two bi-trapezoidal plates. The procedure is outlined in Chapter II.

An explanation of the symbols used for the input data appears below:

NT - number of measuring stations on half the cross section.

T(IZ)- thickness of the plate at measuring station IZ

E - edge thickness of the plate

NI - NT - 1

TT(JK) - thickness of the plate midway between measuring station JK and JK + 1.

YM - Young's Modulus x 10^{-6}

SMU - Poisson's ratio

HTT - half maximum plate thickness

BB - the square of half the plate width

OK - k

DG - distance between measuring stations

RF - range factor of the digital data processor (1.0 when the strain is in micro inches per inch)

I(K) - initial strains read with the plate on a flat surface

J(LK)- strains recorded under load

CC - E

FLA - lambda value.

The strains on one half of the cross section were recorded; first the upper side starting from the plate center then the lower side again starting from the center. The strains on the other half were then recorded in a like manner. Since there were 26 gauges on half the cross section, gauges 1 and 14 were on the top and bottom sides, respectively, at the cross section center. These number 1 and 14 gauges were re-read in recording the second half of the cross section.

```
      DIMENSION G(30),T(15),C(20),S(20),W(20),WT(20),WO(20),F(20),TT(20
      DIMENSION CA(20),EXB(20),SXB(20)
      DIMENSION I(30),J(30)
      READ(5,4) NT,TO,(T(IZ),IZ=1,NT)
    4 FORMAT (I5,F8.5/(10F7.4))
      READ(5,7) E,NI,(TT(JK),JK=1,NI)
    7 FORMAT (F8.5,I5/(10F7.4))
      READ(5,5) YM,SMU,HTT,BB,OK,DG,RF
5     FORMAT (5F7.3,F7.5,F7.3)
2     READ(5,55) (I(K),K=1,26)
55    FORMAT ((13I5))
      READ(5,56) (J(LK),LK=1,26)
56    FORMAT ((13I5))
      READ(5,47) CC,FLA
47    FORMAT(2F7.3)
      DO 57 KM=1,26
      RI=I(KM)
      RG=J(KM)
57    G(KM)=(RG-RI)*RF
      RAD=SQRT(3.*(1.-SMU*SMU))*BB/(FLA*FLA*TO)
      DO 8 II=1,13
      EXB(II)=(G(II)-G(II+13))/2.
      SXB(II)=YM/(1.-SMU*SMU)*(EXB(II)+SMU*1.0E06*T(II)/(2.*RAD))
    8 C(II)=(G(II)-G(II+13))/T(II)
      S(1)=0.
      DO 9 L=2,13
    9 S(L)=S(L-1)+0.5*DG*(C(L)+C(L-1))
      W(1)=0.
      DO 11 M=2,13
11    W(M)=W(M-1)+.5*DG*(S(M)+S(M-1))
      SCA=0.0
      A=SQRT(BB)*(TO+E)
      NB=NI-1
      DO 19 NJ=2,NB
      CA(NJ)=TT(NJ)*(W(NJ)+W(NJ+1))
19    SCA=SCA+CA(NJ)
```

```
      WBA=0.5*DG*(TT(1)*(W(1)+W(2))+SCA+TT(NI)*(W(NI)+W(NI+1)))
      WB=WBA/A
      DO 13 IA=1,13
   13 WT(IA)=W(IA)-WB
      B=CC/(2.*TO)
      DO 15 NN=0,12
      BJ=NN
      BN=12.0
      GAMK=(1.-BJ/BN+B)*TO*(1.+OK)-OK*CC/2.
      CONT=TO*(2.*(1.+OK)/3.+1.*B*(2.+OK)+2.*B*B)/(2.*B+1.)
   15 WC(NN+1)=(GAMK-CONT)*(-1.0)
      DO 17 NA=1,13
      F(NA)=((1.0E-06)*WT(NA)+WO(NA))/HTT
   17 CONTINUE
      WRITE (6,99) FLA,(F(JJ),JJ=1,13)
   99 FORMAT(8H LAMBDA=,F7.3/(1X,5F10.6))
      WRITE (6,98) (SXB(LZ),LZ=1,13)
   98 FORMAT(17H BENDING STRESSES/(1X,5F12.2))
      GO TO 2
      END
```

APPENDIX III

DETAILS OF CARD PUNCH USE

An IBM 024 key punch (card punch) was used to record the strains which were measured by the digital data processor. Figure A3-1 shows the modifications and electrical connections to the key punch necessary for operation with the processor. The connections shown were wired to a "Cannon" connector which was plugged into the key punch outlet in the processor. The numbers shown in figure A3-1 refer to those on the terminal board of the punch and are shown again on IBM Wiring Diagram No. 228001P.

In order for the cards punched to be compatible with the program of Appendix II a drum card for the IBM 024 was used. This card is shown in figure A3-2. With this card thirteen channels of information were recorded per data output card.

[illegible]

[illegible]

[illegible]

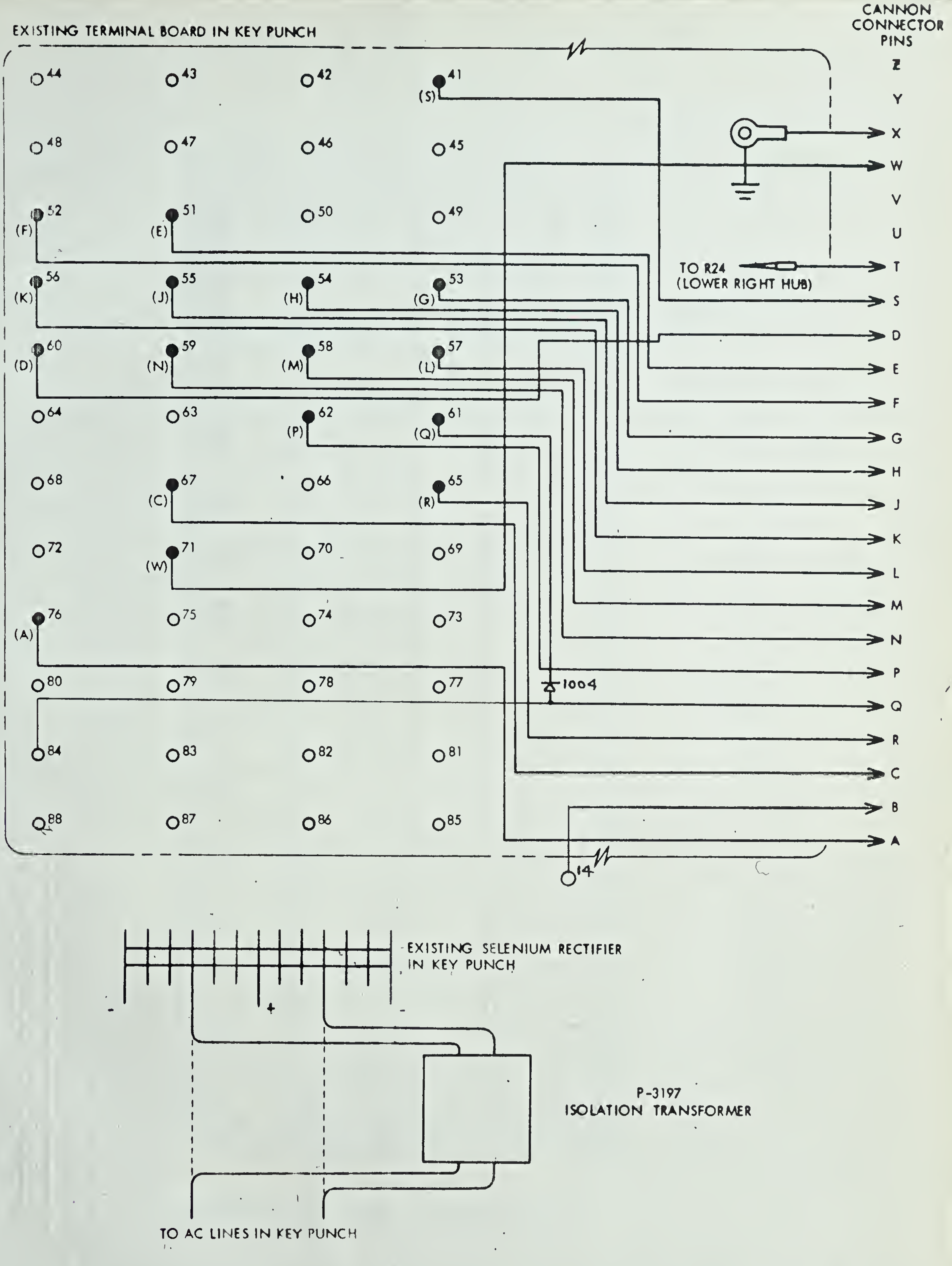

FIGURE A3-1 KEY PUNCH TERMINAL PANEL MODIFICATION

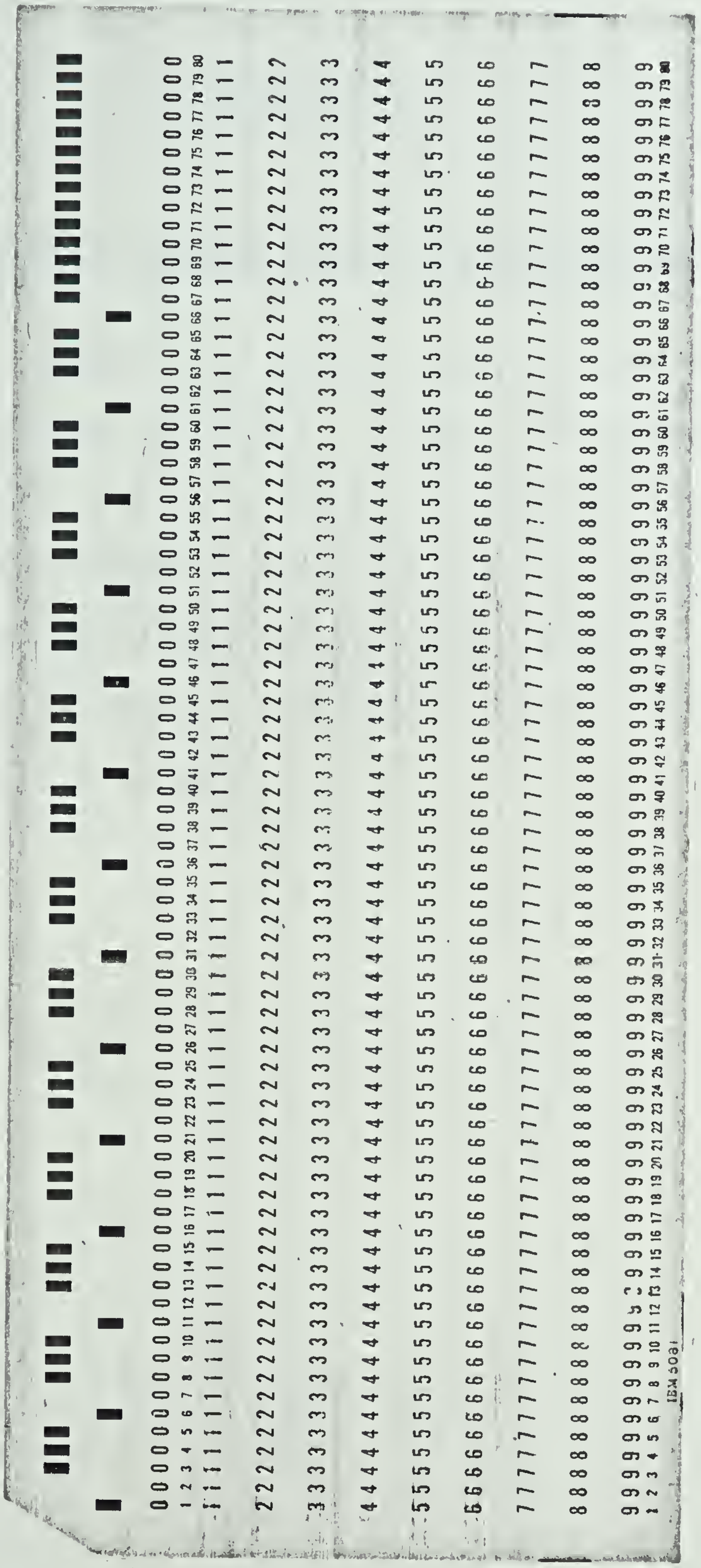

FIGURE A3-2 IBM 024 DRUM CARD

APPENDIX IV

MEASUREMENT OF MOMENT VERSUS CURVATURE RELATION

The moments required to produce the curvatures were measured and recorded. These are shown in figures A4-1 and A4-2. Due to eccentricities in the loading apparatus, the moments recorded are only approximate. The moment needed to counterbalance the weight of the plate to bring the curvature initially to zero has been subtracted from all values.

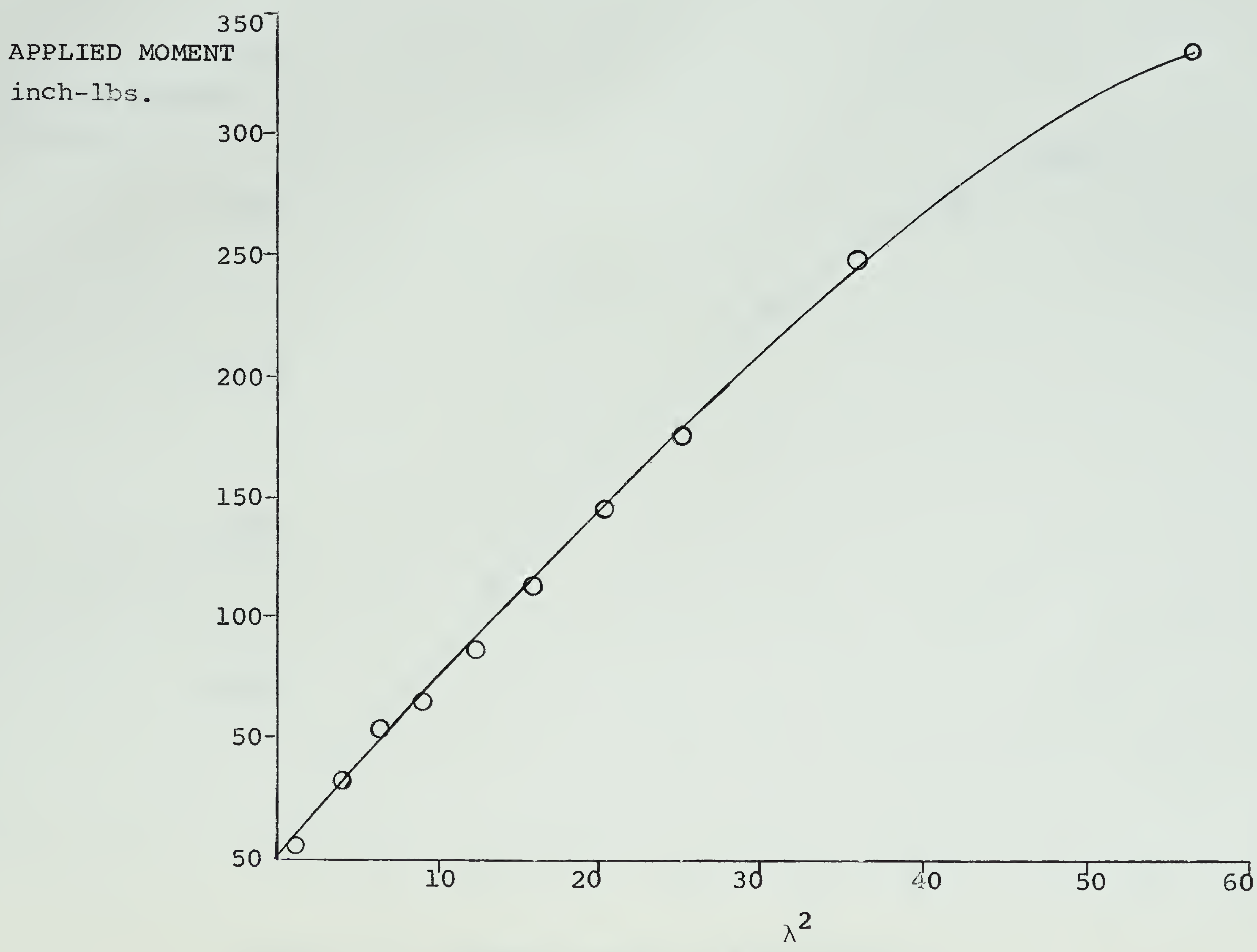

FIGURE A4-1. MOMENT VERSUS λ^2 FOR PLATE I

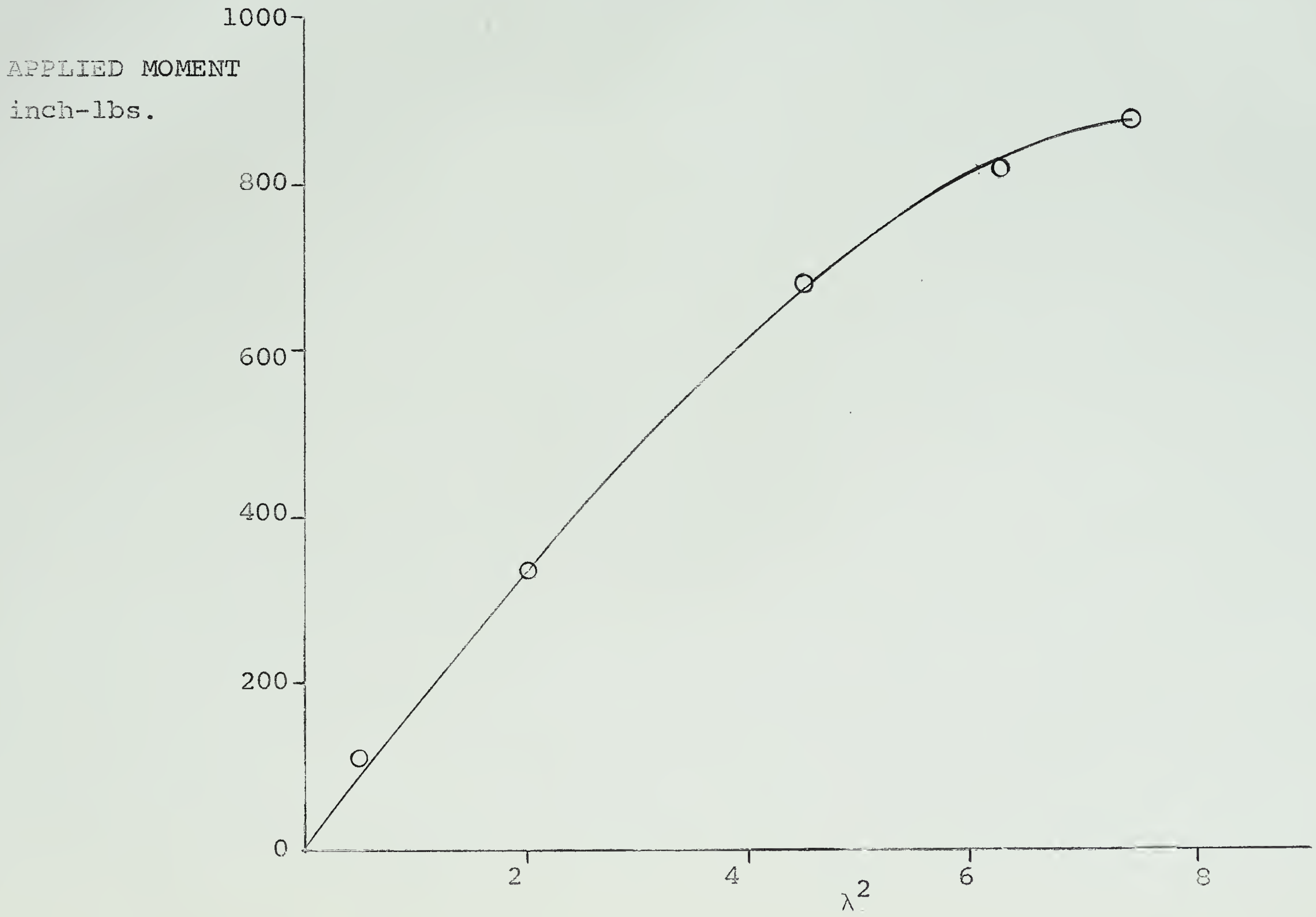

FIGURE A4-2. MOMENT VERSUS λ^2 FOR PLATE II